AD NUMBER

AD859807

LIMITATION CHANGES

TO:

Approved for public release; distribution is unlimited.

FROM:

**Distribution authorized to U.S. Gov't. agencies and their contractors;
Administrative/Operational Use; JUL 1969. Other requests shall be referred to Army Aviation Materiel Labs., Fort Eustis, VA.**

AUTHORITY

USAAMRDL ltr 23 Jun 1971

AD

USAAVLABS TECHNICAL REPORT 69-46

AN INVESTIGATION OF THE LATERAL/DIRECTIONAL DYNAMIC STABILITY CHARACTERISTICS OF A TILT-WING V/STOL TRANSPORT MODEL IN SIMULATED LOW-SPEED DESCENDING FLIGHT

By

William F. Putman

July 1969

U. S. ARMY AVIATION MATERIEL LABORATORIES
FORT EUSTIS, VIRGINIA

CONTRACT DAAJ02-67-C-0025

DEPARTMENT OF AEROSPACE AND MECHANICAL SCIENCES
PRINCETON UNIVERSITY
PRINCETON, NEW JERSEY

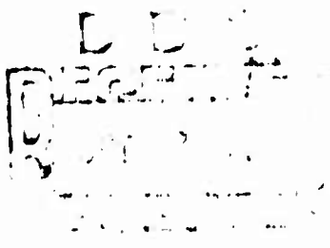

'74

DISCLAIMERS

The findings in this report are not to be construed as an official Department of the Army position unless so designated by other authorized documents.

When Government drawings, specifications, or other data are used for any purpose other than in connection with a definitely related Government procurement operation, the United States Government thereby incurs no responsibility nor any obligation whatsoever; and the fact that the Government may have formulated, furnished, or in any way supplied the said drawings, specifications, or other data is not to be regarded by implication or otherwise as in any manner licensing the holder or any other person or corporation, or conveying any rights or permission, to manufacture, use, or sell any patented invention that may in any way be related thereto.

Trade names cited in this report do not constitute an official endorsement or approval of the use of such commercial hardware or software.

DISPOSITION INSTRUCTIONS

Destroy this report when no longer needed. Do not return it to the originator.

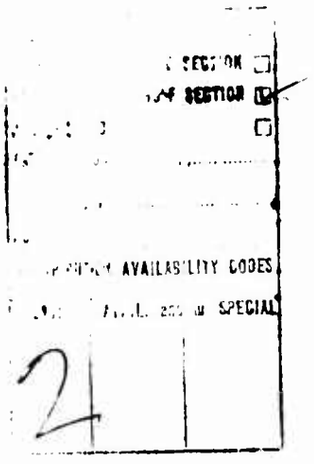

DEPARTMENT OF THE ARMY
HEADQUARTERS US ARMY AVIATION MATERIEL LABORATORIES
FORT EUSTIS, VIRGINIA 23604

This report has been reviewed by the U. S. Army Aviation Materiel Laboratories, the Naval Air Systems Command, and the Air Force Flight Dynamics Laboratories. It is considered to be technically sound.

This work, which was performed under Contract DAAJ02-67-C-0025, was undertaken to determine experimentally the lateral/directional dynamic stability characteristics of a 0.1-scale model of the XC-142A V/STOL aircraft in simulated descending flight. The Princeton Dynamic Model Track was used to perform the investigation.

This report is published for the exchange of information and the stimulation of ideas.

Task 1F162204A14233
Contract DAAJ02-67-C-0025
USAAVLABS Technical Report 69-46
July 1969

AN INVESTIGATION OF THE LATERAL/DIRECTIONAL DYNAMIC STABILITY CHARACTERISTICS OF A TILT-WING V/STOL TRANSPORT MODEL IN SIMULATED LOW-SPEED DESCENDING FLIGHT

Final Data Report

Aerospace Sciences Report 862

By

William F. Putman

Prepared by

Department of Aerospace and Mechanical Sciences
Princeton University
Princeton, New Jersey

for

U. S. ARMY AVIATION MATERIEL LABORATORIES
FORT EUSTIS, VIRGINIA

SUMMARY

This report presents the results of an experimental program to measure the lateral/directional dynamic stability characteristics of a tilt-wing V/STOL transport model in simulated descending flight. A 0.1-scale dynamically similar model of the XC-142A V/STOL aircraft was tested on the Princeton Dynamic Model Track in the three degrees of lateral/directional freedom: roll, yaw, and sideslip. The test conditions simulated a full-scale aircraft with wing loading of 70 pounds per square foot (gross weight = 37,400 pounds), flying at approximately 40 knots at a wing incidence of 40 degrees and flap deflection of 60 degrees. The simulated descent conditions encompassed level flight and four sink rates up to approximately 1,000 feet per minute equivalent full-scale sink rate.

Time histories of the lateral/directional transient response of the model in one, two, and three degrees of freedom were measured. Pursuant to these experiments, the aerodynamic forces and moments acting on the model were measured as functions of the flight variables and model control displacements. The results of these tests defined the descent trim conditions and determined the model control effectiveness and control mixing requirements for this mid-transition flight condition.

Throughout the lateral/directional dynamic test program, the model was stability-augmented in pitching freedom only. A pitch attitude-hold loop, employing pitch rate, pitch attitude, and integral of pitch attitude feedback signals, was used to insure that no spurious lateral/directional motions would occur in the axis system of measurement due to untrimmed body-axis pitching moments. Earlier studies of the lateral/directional motions of this aircraft had indicated the necessity of such a pitch-trim system.

FOREWORD

This research was performed by the Department of Aerospace and Mechanical Sciences, Princeton University, under the direction of Professor H. C. Curtiss, Jr., and the sponsorship of the United States Army Aviation Materiel Laboratories Contract DAAJ02-67-C-0025, Task 1F162204A1'.233, with guidance and financial support from the United States Navy, Naval Air Systems Command, and the United States Air Force Flight Dynamics Laboratory. The research was monitored by Mr. Robert P. Smith of the United States Army Aviation Materiel Laboratories.

The research was performed by Messrs. W. F. Putman, J. J. Traybar, and J. P. Kukon of the Flight Mechanics Laboratory, Princeton University.

BLANK PAGE

TABLE OF CONTENTS

LIST OF ILLUSTRATIONS

LIST OF SYMBOLS

BL	butt line (lateral distance from center line of airplane), inches
c	propeller blade chord, feet
cg	center of gravity of pivoting mass of model
F.S.	fuselage station (horizontal reference), inches
F	resultant aerodynamic force acting on model, pounds
g	acceleration due to gravity, feet per second squared
I_x, I_z	model moments of inertia about principal axes, slug-feet squared
I_x', I_z', I_{xz}'	model moments of inertia and product of inertia about space axes, slug-feet squared
i_w, i_t	wing incidence and tail incidence, respectively, degrees
k_{Ψ_m}	mechanical spring constant in yaw, foot-pounds per radian (negative for normal spring restoring moment sense)
L	model aerodynamic rolling moment, foot-pounds
L_p, L_r, L_v	stability derivatives, rate of change of rolling moment divided by inertia I_x with variable indicated in subscript
ℓ	longitudinal instrumentation proportionality constant, feet
m	equivalent aerodynamic mass of model, slugs ($m = \frac{F}{g}$ slugs)
m_ℓ	mass of lateral travel link, slugs ($m_\ell = 0.17$ slug)
m_p	pivoting mass of model, slugs ($m_p = 1.57$ slugs)
m_t	total mass accelerated by the model when translating laterally, slugs ($m_t = m_p + m_\ell$)
$\frac{m}{m_t}$	ratio of equivalent aerodynamic mass of model to lateral translating mass
N	yawing moment about Z (principal) axis, foot-pounds

N_p, N_r, N_v	stability derivatives, rate of change of yawing moment divided by inertia I_z with variable indicated in subscript
p	model angular velocity in roll about principal axis, radians per second or degrees per second ($p = \dot{\phi} \cos \zeta - \dot{\Psi} \sin \zeta$)
PVC	polyvinyl chloride plastic
q	model angular velocity in pitch about principal axis, radians per second or degrees per second ($q = \dot{\theta}$)
R	propeller blade radius, feet
r	distance along propeller radius (measured from axis of rotation), feet; or model angular velocity in yaw about principal axis, radians per second or degrees per second ($r = \dot{\Psi} \cos \zeta + \dot{\phi} \sin \zeta$)
$\frac{r}{R}$	propeller blade radial station
rpm	model propeller rotational speed, revolutions per minute
t	propeller blade thickness, feet
T_{tr}	tail rotor thrust, pounds
U	aircraft velocity along body-fixed X"-axis (principal axis system), feet per second
U_f	aircraft horizontal velocity (space-fixed axis system), feet per second, $U_f = U_{o_f} + U_f$
U_o	aircraft initial velocity along X"-axis (principal axis), feet per second
U_{o_f}	aircraft initial horizontal velocity (space-fixed axis system), feet per second
u_f	aircraft horizontal perturbation velocity (space-fixed axis system), feet per second
V_f	aircraft lateral velocity (space-fixed axis system), feet per second
V_{o_f}	aircraft initial lateral velocity (space-fixed axis system), feet per second
v	aircraft lateral perturbation velocity along body-fixed Y"-axis (principal axis system), feet per second

V	aircraft velocity along body-fixed Y"-axis (principal axis system), feet per second
v_f	aircraft lateral perturbation velocity (space-fixed axis system), feet per second
W	model weight, pounds; or aircraft velocity along body-fixed Z"-axis (principal axis system), feet per sec. d
W_f	aircraft vertical velocity (space-fixed axis system), feet per second
W_p	model pivoting weight, pounds (W_p = 45.9)
W_{o_f}	aircraft initial vertical velocity (space-fixed axis system), feet per second
W_o	aircraft initial velocity along body-fixed Z"-axis (principal axis system), feet per second
w_f	aircraft vertical perturbation velocity (space-fixed axis system), feet per second
W.L.	water line (vertical distance from airplane horizontal reference plane), inches
X	aerodynamic force acting along $\bar{X}$ -axis, pounds, positive forward
X', X"	model gimbal roll axis
X_f	longitudinal horizontal axis (space-fixed axis system) and force acting along X_f axis at γ = 0
$\bar{X}$	longitudinal body axis (principal axis system)
x_{cg}	longitudinal position of model cg, percent mean aerodynamic chord at i_w = 0
Y	aerodynamic force acting along $\bar{Y}$-axis, pounds, positive to starboard
Y', Y", $\bar{Y}$	body-fixed lateral axis (principal axis), coincides with model gimbal pitch axis
Y_f	lateral axis (space-fixed axis system) and force acting along Y_f axis at γ = 0
Y_v	stability derivative, rate of change of lateral horizontal force divided by mass m with lateral velocity, per second, body axis and space axis system

Z	aerodynamic force acting along Z-axis, pounds, positive downward (principal axis system)
Z''	body-fixed vertical axis (principal axis system)
Z_f	vertical axis (space-fixed axis system) aligned with gravity and aerodynamic force acting along Z_f-axis, pounds
$\bar{Z}_f$	vertical space axis, coincides with model gimbal axis
z_{cg}	vertical distance of model cg from wing reference plane, percent mean aerodynamic chord
α	angle of attack, degrees
β	local propeller blade angle, degrees
$\beta_{.75R}$	average propeller blade angle (collective pitch) measured at the three-quarter radius and averaged for four propellers, degrees
ΔN_{Ψ_m}	additional stability derivative due to mechanical spring in yaw, per second squared
$\Delta\beta_p$, $\Delta\beta_s$	differential collective pitch on port and starboard propellers, respectively (averaged for two propellers), degrees
γ	descent angle, degrees (position for climbing flight)
δ_a	aileron deflection, degrees (positive for aileron trailing edge forward with wing at 90 degrees incidence)
δ_f	flap deflection, degrees
ζ	inclination of X" (principal) axis to horizontal plane, degrees or radians, $\zeta = \theta - \eta$, positive nose up
η	angle between model principal axis and fuselage reference line, degrees (positive for principal axis inclined downward)
θ	fuselage pitch attitude, degrees or radians, positive nose up
λ	linear scale factor, $\lambda = \frac{\text{model length}}{\text{full-scale length}}$
ϕ	roll angle about model gimbal roll axis, degrees or radians
Ψ	yaw angle about model gimbal yaw axis, degrees or radians
$\dot{(\ )}$	differentiation with respect to time
$(\ )'$	perturbed locations of axes

$(\bar{\ })$	vector
$(\ )_p$	control on port side of airplane
$(\ )_s$	control on starboard side of airplane
$(\ )_{\dot{\phi}}$, $(\ )_{\dot{\psi}}$	gimbal axis stability derivatives, rate of change of moment about gimbal axis with variable indicated in subscripts, foot-pound-seconds
$(\ )_{v_f}$	space axis stability derivative, rate of change of moment about gimbal axis with space-fixed axis system lateral velocity, pound-seconds

BLANK PAGE

INTRODUCTION

Tilt-wing V/STOL aircraft have typically experienced deteriorating lateral/directional handling qualities in low-speed flight conditions at steep descent angles.[1,2,3,4] These flight conditions have been simulated with dynamically similar models free-flown in a wind tunnel, and additional qualitative information has been obtained on the flight behavior of the aircraft by means of such model experiments.[3] Steep-descent wing stall phenomena, which are thought to be a factor in the aircraft's handling qualities, have been investigated on several tilt-wing configurations[5,6] in wind tunnels. These tests have produced quantitative information on the aerodynamic forces and moments acting on the aircraft and have provided visualization of the airflow by means of tufts. Correlation was obtained between handling-qualities-limited descent boundaries observed on a free-flight model and wing stall conditions as evidenced by tuft patterns on a similar model.

Direct quantitative measurements have been made of both the static and the dynamic lateral/directional stability characteristics of the XC-142A, a tilt-wing V/STOL configuration, in level, low-speed flight using a dynamically similar model.[7] These tests indicated that the aircraft, although exhibiting dynamically unstable modes of motion, was well behaved, in that the motions could be characterized by a conventional set of linear equations of motion. It would be expected that such an aircraft with reasonable control effectiveness and with conventional stability augmentation would exhibit satisfactory handling qualities.

A series of experiments was undertaken on the Princeton Dynamic Model Track to study the lateral/directional dynamic stability characteristics of a 0.1-scale dynamically similar model of the XC-142A tilt-wing V/STOL aircraft at various trim conditions simulating low-speed descending flight. The trim conditions were determined from preliminary experiments in which the forces acting on the aircraft were measured as functions of power setting and flight condition. Based on these data, a dynamic test program was designed to provide quantitative measurements of the lateral/directional transient response time histories of the aircraft in various lateral/directional degrees of freedom and to measure the lateral and directional control effectiveness.

DESCRIPTION OF TEST APPARATUS

The Princeton Dynamic Model Track, as described in Reference 8, is a unique facility that allows the direct measurement of low-speed aircraft dynamic stability characteristics through the use of dynamically similar models. The principal piece of apparatus that permits the direct measurement of dynamic characteristics is a main dynamic carriage that can follow the longitudinal velocity excursions of the model. However, for lateral/directional experiments, the main dynamic carriage is not used in the model-following capacity, but rather is programmed to run at a constant velocity.

CARRIAGE

The lateral velocity excursions of the model are provided for by means of the lateral servo boom attachment to the main carriage as in Figure 1. This arrangement allows a maximum of 8 feet of sideslip excursion. A small error carriage follows the model lateral motions to prevent large relative velocities between the model and the main carriage, thereby reducing bearing friction. This error carriage is driven by an on-off servo actuated by microswitches; the servo is rate-limited at approximately 10 feet per second, allowing a full-scale-excursion bandwidth of more than 2 radians per second.

CONTROLS AND COMPUTER

In addition to the normal complement of carriage and model control apparatus carried on the main carriage, an analog computer has been added since the experiments of Reference 7. This computer, with 10 uncommitted patchable amplifiers, permits stability-augmented model operation and provides signal conditioning for various control and instrumentation channels.

MODEL

A photograph of the 0.1-scale dynamically similar model is presented in Figure 2, and a general arrangement drawing is shown in Figure 3. The model is the same as the one used in Reference 7 but with several modifications. The wing leading-edge Krüger flaps, in place for the experiments of Reference 7, have been replaced by conventional slats as shown in Figure 4. Just as with the Krüger flaps, the slats were located behind only the upcoming propeller blades, as indicated in Figure 5.

Other modifications to the model were mainly associated with the control system and included increased tail rotor control power, tail rotor thrust measurement instrumentation, and increased bandwidth on tail rotor, aileron and collective pitch actuation systems. These control system improvements were made to allow stability augmentation loops to be closed about various model degrees of freedom.

The model lateral/directional control system is similar to that of the full-scale XC-142A aircraft. In hovering flight (wing incidence near 90°), ailerons operating in the propeller slipstream are used for yaw control, and roll control is provided by differential propeller pitch; in forward flight (wing incidence near zero), the ailerons assume their conventional role as roll controls while yawing moment is provided by the rudder. The model was designed exclusively for low-speed testing, and therefore rudder control was not provided. Intermediate-wing-incidence yawing moment control is produced by linear combinations of aileron and differential propeller blade pitch. This mixing is accomplished electrically (by means of the analog computer mentioned previously) and, for a given model operating condition and configuration, allows pure body-axis rolling moment and yawing moment to be generated by linearly independent controllers.

The geometric characteristics of the model propeller blades are presented in Figure 6 and are not precisely scaled since they were fabricated using the outboard portion of blade molds from a 0.11-scale model.

Model aileron geometry is shown in Figure 4; the ailerons are exactly scaled except that the trailing-edge cusp of the NACA 63-318 airfoil is retained and the gap seal technique is unconventional. The aileron gap seal was provided in the model aileron system by means of strips of 1-mil sheet plastic taped to either side of the aileron gap on the wing lower surface, as shown in the detail inset of Figure 4. More conventional rubbing-type seals were unsatisfactory because of the high friction level associated with them, and the unsealed ailerons exhibited poor aerodynamic characteristics which were greatly improved by the use of gap seals.

MODEL SUPPORT AND GIMBAL SYSTEM

The model support system, shown schematically in Figure 7, includes a set of gimbals that allows particular degrees of angular freedom to be selected. Those angular degrees of freedom that are not under investigation are locked out by means of disc-type brakes, which also serve to arrest the model motions at the end of a run. The gimbal and the support system also serve as references for measurement of the model motions.

The gimbal system is similar to the one used in Reference 7 with the yaw axis fixed to the lateral error linkage; the roll axis yaws with the model, and the pitch axis is fixed to the model. For the present experiments, the descent conditions were simulated by pitching the model nose-up for increased fuselage angle of attack.

The exact expressions for the variables and the pertinent equations of motion for the measurement axis system are presented in the appendix; however, it should be noted here that the roll and yaw axes do not pitch with the model.

INSTRUMENTATION

The basic test instrumentation is similar to that used in the tests of Reference 7, employing telemetering and magnetic tape recordings; however several additions and refinements have been made to the model instrumentation.

The model support tube, shown in Figure 7, was strain-gage instrumented for bending moments about the longitudinal and lateral axes and for torsion about the vehicle axis. With proper testing technique this instrumentation permitted the measurement of all six free-body forces and moments. Additionally, the tail rotor support member was instrumented for measurement of tail rotor thrust, a feature that was only incidental to the subject tests.

A package consisting of three miniature rate gyros was installed in the model to measure the angular rates about three mutually perpendicular body axes. The vertical axis was located in the plane of symmetry, and the longitudinal axis was aligned with the model principal axis.

DISCUSSION OF PROCEDURES AND RESULTS

STATIC TESTS

Static testing refers to all types of tests in which the principal measurements made were of forces and/or moments acting on the model. The description "static" does not mean at zero velocity, as in hover, but, rather, as opposed to dynamic tests where the principal measurements were of the flight variables such as attitudes and velocities.

The static tests included not only force and moment measurements to determine descent conditions but also control effectiveness and control mixing tests. For some of these tests, particularly the control mixing tests, dynamic model freedoms were allowed as part of the experiment, but the tests are still referred to as static since their principal aim was not the determination of the model's dynamic characteristics.

Stability Augmentation System

The instrumentation on the model support tube was used to measure the aerodynamic forces and moments acting on the model. Since this instrumentation system was capable of measuring only moments about three mutually perpendicular axes, it was necessary to arrange the experiments so that the forces and moments could be measured separately. This was accomplished by closing a stabilizing feedback control loop around the particular rotational degree of freedom (notably pitch or roll) and allowing the model to fly free in that degree of freedom. Thus,the moment acting on the model was guaranteed to be zero, and any bending strain observed by the instrumentation was due to a force applied through the model gimbal axis. For example, throughout the test program, the model was always free in the pitching degree of freedom, and the proper aircraft attitude was insured by a pitch attitude loop closure utilizing pitch attitude, the integral of pitch attitude, and pitch rate signals to command tail rotor collective pitch. Thus, the airplane pitching moment about the pitch gimbal axis was necessarily zero, a condition that was shown to be desirable in the analysis of Reference 7. Moreover, any bending strain observed in the model support tube longitudinal moment axis (assuming no interactions) must be due to an axial force (X_f-force) applied through the model pitch gimbal. Similarly, an attitude stabilization loop was closed around the rolling degree of freedom, and a side force (Y_f-force) was measured with the support tube lateral moment instrumentation. The yawing moment was measurable directly by means of the model support tube torque instrumentation.

As a preliminary step to performing the actual descent tests,it was necessary to make several series of test runs to establish the proper descent test conditions. The earliest runs were devoted to establishing the high-performance pitch attitude-hold loop discussed above; a time history of a typical pitch attitude loop transient response is presented in Figure 8.

Aileron Effectiveness Tests

Aileron effectiveness tests were conducted for the dual purposes of linearizing the control characteristics and measuring the magnitude of the rolling and yawing moments as functions of aileron deflection. Since the aileron system is in fact the major portion of the outboard flaps (Figure 4), the aileron effectiveness and linearization tests serve to indicate, qualitatively, the flap effectiveness.

At a flap deflection, δ_f, of 60 degrees, the full-scale airplane ailerons actuate consecutively rather than simultaneously; that is, as the aileron controller is moved from one stop toward the other, one aileron on one wing will move from a negative δ_a (Figure 4) toward $\delta_a = 0$ while the aileron on the other wing remains at zero deflection. At the point where the first aileron is at zero deflection, the other aileron commences to deflect from zero toward a negative deflection. A similar aileron deflection program was used on the model; limiting and sequencing of the controls were accomplished electrically in the analog computer using biased diode circuits.

Typical results of the control effectiveness are shown in Figures 9 through 11. All of the data presented in Figures 9 through 11 have been replayed through second-order filters with natural frequencies of approximately 5 radians per second and damping ratios of approximately 0.7. Although the control data channels had little noise in them, they also were filtered to maintain time synchronization with the other channels; the control input profiles were actually sharp-cornered as noted. Figure 9 is a time history of the longitudinal force, X, rolling moment, L, and yawing moment, N, as functions of the aileron deflections indicated. The linearity of the resulting yawing moment with control deflection is evident; however, it should be noted that a slight overlap of the port and starboard controls was necessary to achieve this linearity. Also to be noted is the nonlinear rolling moment generated at this wing-flap condition by aileron deflection and the effect of consecutive aileron deflection on longitudinal force, X. Figure 10 shows the same quantities as functions of differential propeller blade pitch, $\Delta\beta$. It can be seen that this control, at a wing incidence of 40 degrees and a flap deflection of 60 degrees, produces significant yawing moments as well as rolling moments; however, there is no net force change apparent in the X-force channel.

To provide a pure rolling moment with a single controller, it was necessary to mix a proportional amount of aileron deflection with differential propeller blade pitch. The required ratio of aileron to blade pitch that would just cancel the yawing moment produced by the differential blade pitch was determined experimentally. A typical experimental result is presented in Figure 11, which shows a time history of force and control moments as functions of the mixed control inputs.

Descent Conditions

The specific test conditions used to simulate the aircraft in descending flight were determined from static test measurements of lift and drag forces. Figure 12 demonstrates the basic force components that were measured and their geometric relation to the desired forces; lift was measured by rolling the model about the model gimbal roll axis and measuring the space axis Y = force, and drag was measured by means of the space axis X_f -force instrumentation.

As explained in the discussion of the model instrumentation, the model support tube instrumentation measured the bending moment in the model support tube; to obtain the X_f and Y_f forces, it was necessary to insure that the bending moments about the model gimbal roll and pitch axes were zero. This was accomplished by closing the pitch and roll attitude stabilization loops which maintained the gimbal axis moments at zero. With these loops closed, the model support tube instrumentation read as follows (at $\Psi = 0$):

1. Side force gage; $Y_f = (\text{lift}) \sin \phi$

and

2. Longitudinal force gage; $X_f = (\text{drag}) - \frac{N}{\ell} \cos \theta \sin \phi$,

where X_f and Y_f are space axis forces, lift and drag are conventional wind axis forces, and N is the body-axis yawing moment. The yawing moment term appears because of the resolution of the body-axis moment onto the space axis instrumentation; the constant ℓ, with dimensions in feet, was determined by calibration. Since yawing moment, N, was measured independently as torsion in the support tube, the lift and the drag could be uniquely determined from the X_f and Y_f readings in conjunction with measurements of roll angle, ϕ, pitch angle, θ, and yawing moment, N.

The data presented in Figure 13 were obtained by programming a ramp input to the roll attitude loop with the pitch attitude-hold loop closed and with yawing moment trimmed. At $\phi = 0$, the rate of change of the Y_f-force reading with roll angle is the lift force directly, and the X_f-force reading is the drag force, independent of yaw trim.

Figure 14 presents results of a different type of test wherein the pitch angle is programmed to obtain a wide range of trim condition information in the course of a single run. A third type of test, the results of which are presented in Figure 15, utilizes a velocity profile to obtain a wide range of trim condition information. This last type of test is the most difficult to analyze because the X_f-force instrumentation measures the reaction to the force required to accelerate the model mass. Unless special mass-balanced instrumentation is used, the data must be corrected for the acceleration effects; this correction has been made for the data presented in Figure 15.

A summary of the test conditions is presented in Figure 16 and in Table I.

DYNAMIC TESTS

The results of the lateral/directional dynamic tests at five descent conditions including level flight are presented in Figures 17 through 38 as time histories of the transient response of the model to random or control inputs as recorded. All tests were performed at a wing incidence of 40 degrees ($i_w = 40^o$), a flap deflection of 60 degrees ($\delta_f = 60^o$), and a model propeller speed of 4000 revolutions per minute (rpm = 4000). Test conditions are summarized in Table I, and the equivalent full-scale flight conditions are presented in Figure 16 in comparison to estimates of descent capability from Reference 3. A listing of the scale factors for the model is given in Table II, and a summary of the model geometric and inertial characteristics is presented in Table III.

The data of Figures 17 through 38 have been replayed through second-order filters with natural frequencies of approximately 30 radians per second and damping ratios of approximately 0.7. Any data channel not specifically shown in these figures can be assumed to be unchanging with time during the course of the run. A comprehensive treatment of dynamic test data analysis is presented in Reference 9.

Typical test procedure for lateral/directional dynamic testing is to preset the model attitudes and controls at or near the proper position for the particular trim condition. The main carriage is then programmed to accelerate the model to the desired flight speed, at which time the degrees of freedom under investigation are released. The end of the data portion of a run is determined when any model angular excursion reaches its limit or when the carriage/model system passes a braking switch located near the end of the track. At this time the model releases are reengaged, and the carriage/model system is braked to a halt.

Model Trim

The determination of near-perfect model trim is an important requisite for conducting dynamic tests, and the stability augmentation capability is of great value in this determination. Ideally, very "tight" loops could be established around the various degrees of freedom so that the model, when released, would seek its own stable closed-loop trim condition; at this time the controls could be locked, the loops could be opened, and the open-loop transient response would ensue. In practice, however, any control loop with gain sufficiently high to hold the aircraft within tolerable limits of a prescribed attitude is seldom to be found in a quiescent state. As a consequence, the controls are always moving; if, at any instant in time, they are shut off, the aircraft will be out of trim. The solution to this problem can be found in tailoring a low-pass track-and-hold system in parallel with the control position transducer feedback signal; however, experience has indicated that, with limited computer capacity, this can be a development problem in itself. The alternate solutions, and the ones

adopted for these tests, are either to repeat runs until a sufficiently small residual input remains at loop opening or to release the model open loop with the controls preset to the average level indicated by a previous closed-loop run. The first of these two solutions works well when the model dynamics are not too unstable, and a large known input may be applied after release to excite the transient response. However, when the model dynamics are unstable to the degree that it is not possible to excite them with a sizable input, it is preferable to use the latter preset control technique. In either case, the stability augmentation system is of significant benefit in reducing testing time and improving data quality through good trim determination.

Single-Degree-of-Freedom Tests

At each of the five descent conditions investigated, experiments were conducted in a single degree of rotational freedom, ψ. As can be seen in Equation (13) of the appendix, these tests yield very direct information with regard to the important directional stability and yaw damping derivatives.

It is important to note that some of the single-degree-of-freedom tests were performed with a mechanical spring restraining the yawing motion; Table I should be consulted. The spring-restrained single-degree-of-freedom motions are performed both at the flight trim condition and with the model motor off and carriage velocity equal to zero (U_{o_f} = rpm = 0).

The latter case is used for determining the model moment of inertia as well as for estimating the damping due to bearing friction. The model-motor-off value of bearing friction damping so obtained is a maximum value, in that it includes all power-off damping as well as represents the bearing friction with the full weight of the model resting on the gimbal bearings. During a test run, at least a part of the model weight is supported aerodynamically; thus, the bearing friction will be somewhat less than indicated by the power-off experiment.

Multiple-Degree-of-Freedom Tests

At each descent condition, experiments were conducted in two degrees of freedom in roll and yaw (ϕ,ψ), in two degrees of freedom in roll and sideslip (ϕ,v), and in three degrees of freedom in roll, yaw, and sideslip (ϕ,ψ,v). Equations of motion for each of these cases are presented in the appendix. No mechanical springs were used for any of the multiple-degree-of-freedom tests, and for the data presented, only pitching motions were stability-augmented. For all multiple-degree-of-freedom tests, the pitch degree of freedom was free, and the pitch attitude-hold loop was in operation, thereby insuring that the body-axis pitching moment was zero.

TABLE I. SUMMARY OF TEST CONDITIONS

All tests conducted at $i_w = 40°$, $\delta_f = 60°$, $i_t = 20°$, and model rpm = 4000 except where rpm = 0 as noted.

Fuselage Pitch Attitude θ (deg)	Collective Pitch $\beta_{.75R}$ (deg)	Descent Angle γ (deg)	Trim Velocity U_f (ft/sec)	Run Nos.	Figure Nos.	Degrees of Freedom
0	11.5	0	17.4	97 99	17	ψ*
	13.5	0	17.8	87 88	18	
				91	19	
			0	92**		
			19.4	102 106	20	
			17.6	164 166	21	ϕ-ψ
			18.4	179 182	22	ϕ-v_f
			17.9	203 204	23	ϕ-ψ-v_f
10	13.5	-5	17.8	213 214	24	ψ
			17.7	210 212	25	ϕ-ψ
			17.6	220 224	26	ϕ-v
			18.4	228 229	27	ϕ-ψ-v_f

TABLE I - CONTINUED

All tests conducted at $i_w = 40°$, $\delta_f = 60°$, $i_t = 20°$, and model rpm = 4000 except where rpm = 0 as noted.

Fuselage Pitch Attitude θ (deg)	Collective Pitch $\beta_{.75R}$ (deg)	Descent Angle γ (deg)	Trim Velocity U_f (ft/sec)	Run Nos.	Figure Nos.	Degrees of Freedom
20	13.5	-11	18.6	234 235	28	Ψ
				231 232	29	ϕ-Ψ
			18.4	238 239	30	ϕ-v_f
				247 248	31	ϕ-Ψ-v_f
	11.5	-11	18.1	261 263	32	Ψ
			18.8	251 254	33	ϕ-Ψ
			18.4	269 270	34	ϕ-v_f
		-11	23.5	323 326	35	Ψ
			24.0	331 336	36	ϕ-Ψ
			23.6	327 329	37	ϕ-v_f
				339 341	38	ϕ-Ψ-v_f

* Mechanical spring in place, k_{Ψ_m} = -31.7 ft-lb/rad

** rpm = 0

TABLE II. SCALE FACTORS FOR DYNAMIC MODEL SIMILARITY

Multiply full-scale property by scale factor to obtain model property.

		For $\lambda = 0.10$
Linear dimension	λ^1	0.1
Area	λ^2	0.01
Volume, mass, force	λ^3	0.001
Moment	λ^4	0.0001
Moment of inertia	λ^5	0.00001
Linear velocity	$\lambda^{.5}$	0.316
Linear acceleration	λ^0	1
Angular velocity	$\lambda^{-.5}$	3.16
Angular acceleration	λ^{-1}	10
Time	$\lambda^{.5}$	0.316
Frequency	$\lambda^{-.5}$	3.16
Reynolds number	$\lambda^{1.5}$	0.0316
Mach number	$\lambda^{.5}$	0.316

where $\lambda = \frac{\text{model linear dimension}}{\text{full-scale linear dimension}}$

TABLE III. MODEL GEOMETRIC AND INERTIAL CHARACTERISTICS

Model Weight, W_p, = 45.9 pounds

Rolling Moment of Inertia, I_x, = 3.0 slug-feet squared

Yawing Moment of Inertia, I_z, = 4.1 slug-feet squared

Wing Area = 5.34 feet squared

cg Position:

x_{cg} = 9 percent mean aerodynamic chord at $i_w = 0$

z_{cg} = 26.5 percent mean aerodynamic chord below wing reference plane location at $i_w = 0$

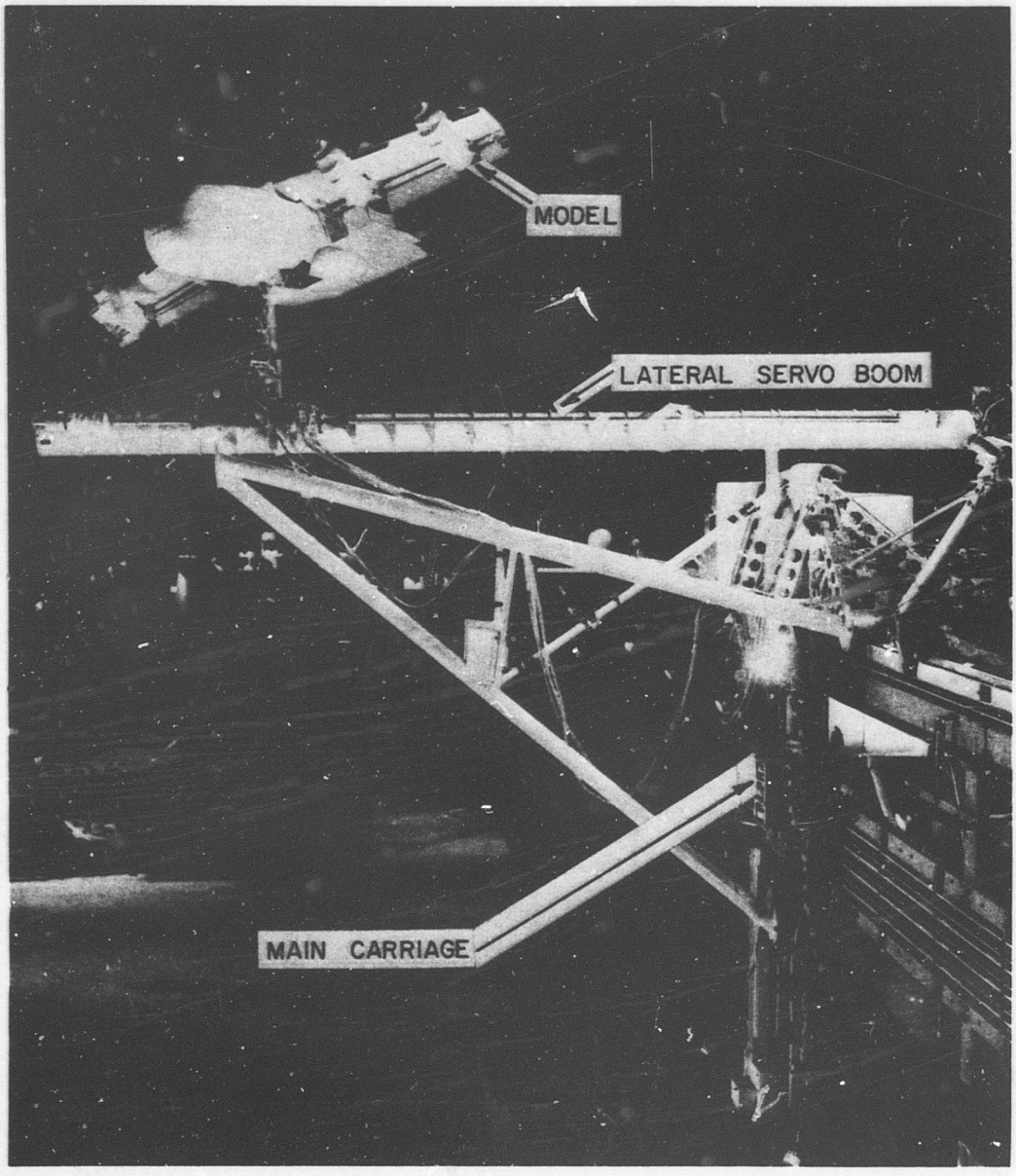

Figure 1. Princeton Dynamic Model Track, Showing Model Mounted on Lateral/Directional Testing Apparatus.

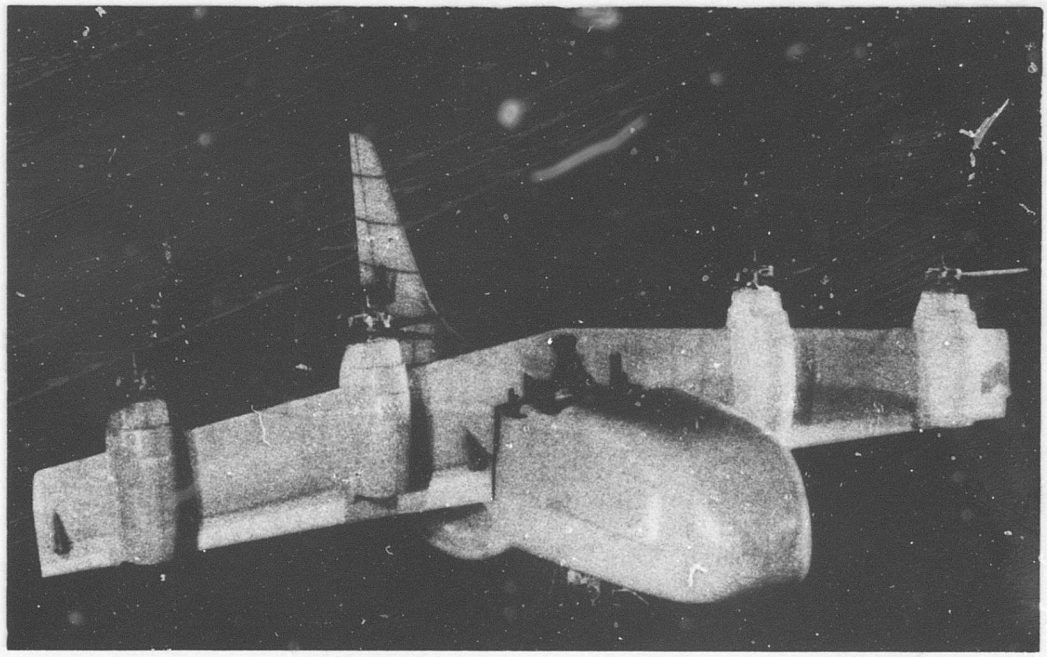

Figure 2. 0.1-Scale Dynamic Model of XC-142A Tilt-Wing V/STOL Aircraft.

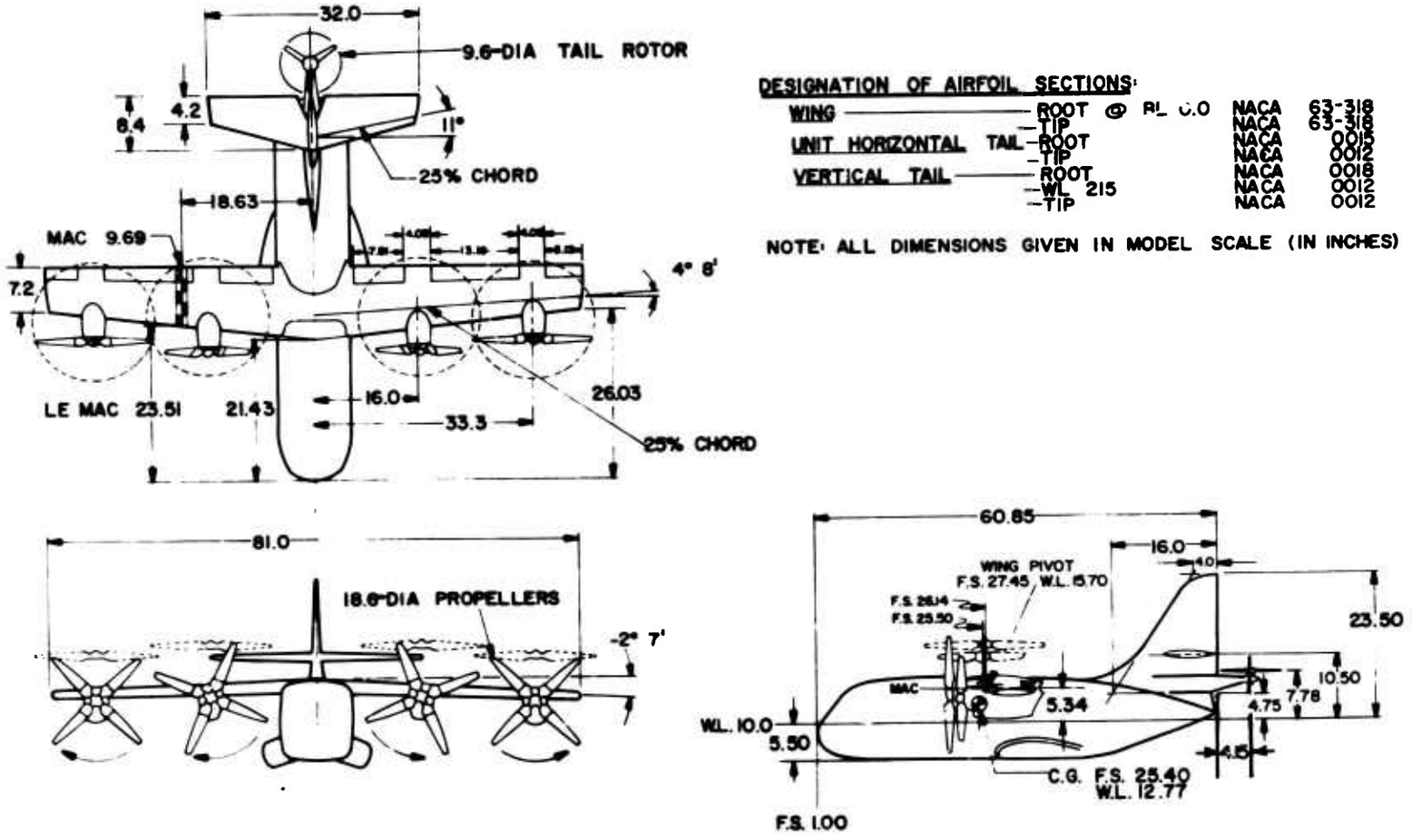

Figure 3. General Arrangement, 0.1-Scale XC-142A Model.

Note. Wing Airfoil Section NACA 63-318
Angular Travel of Vane = 1.075 x Angular Travel at Flap
All Dimensions Given in Percent Chord at Any Wing Station

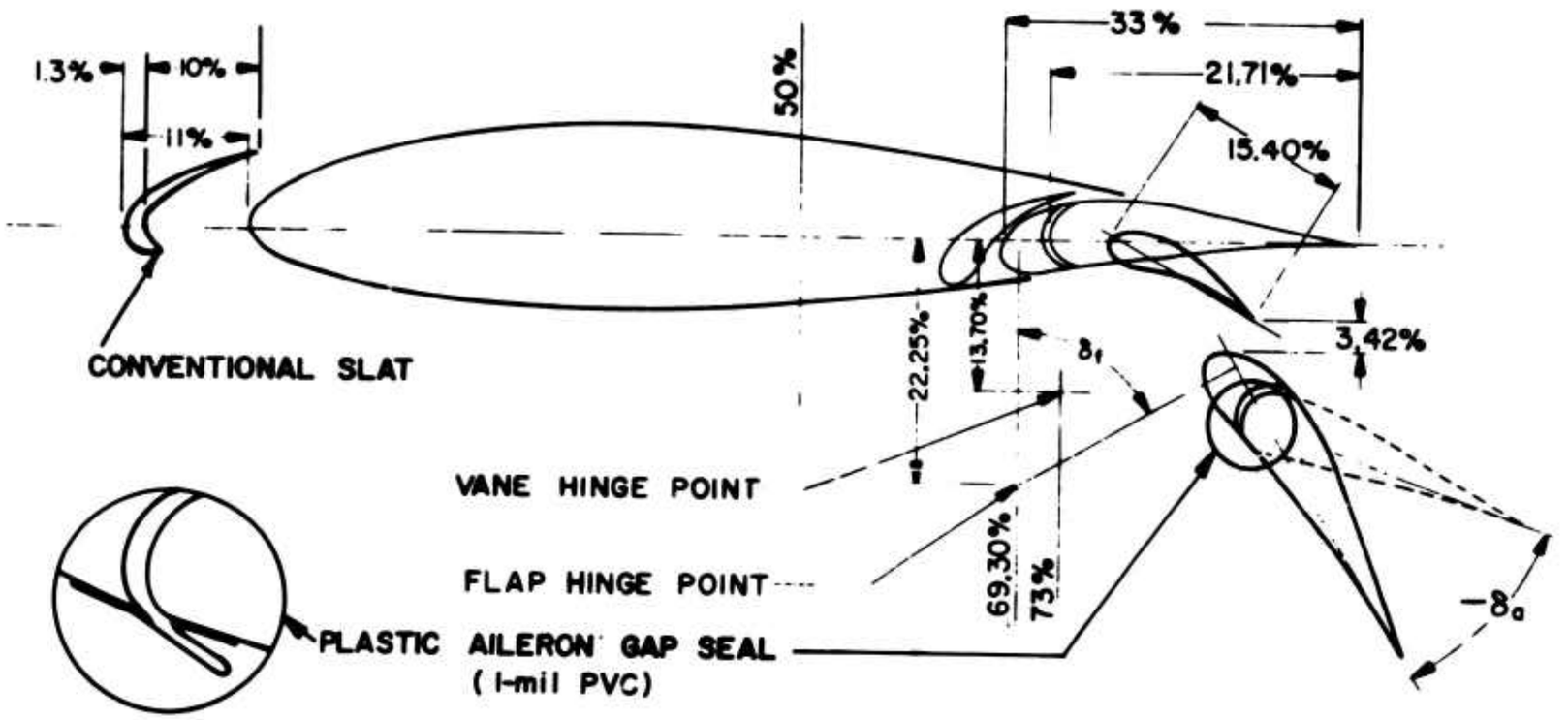

Figure 4. Model Wing Airfoil Section, Showing Slat, Flap, and Aileron Arrangement.

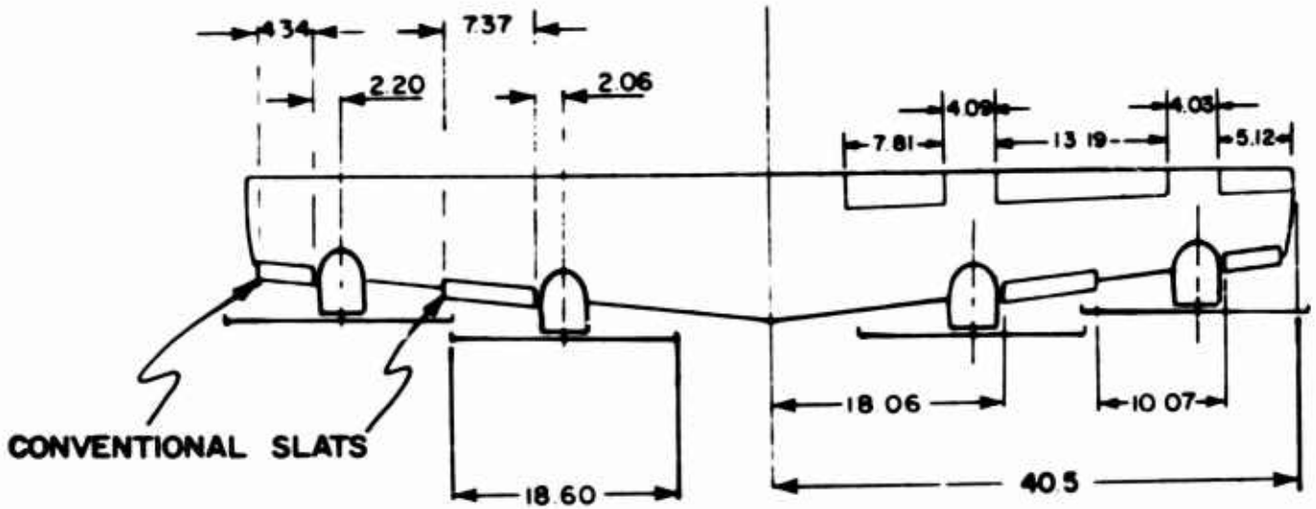

Note: All dimensions are in inches.

Figure 5. Model Wing Plan Arrangement Showing Spanwise Flap and Slat Locations.

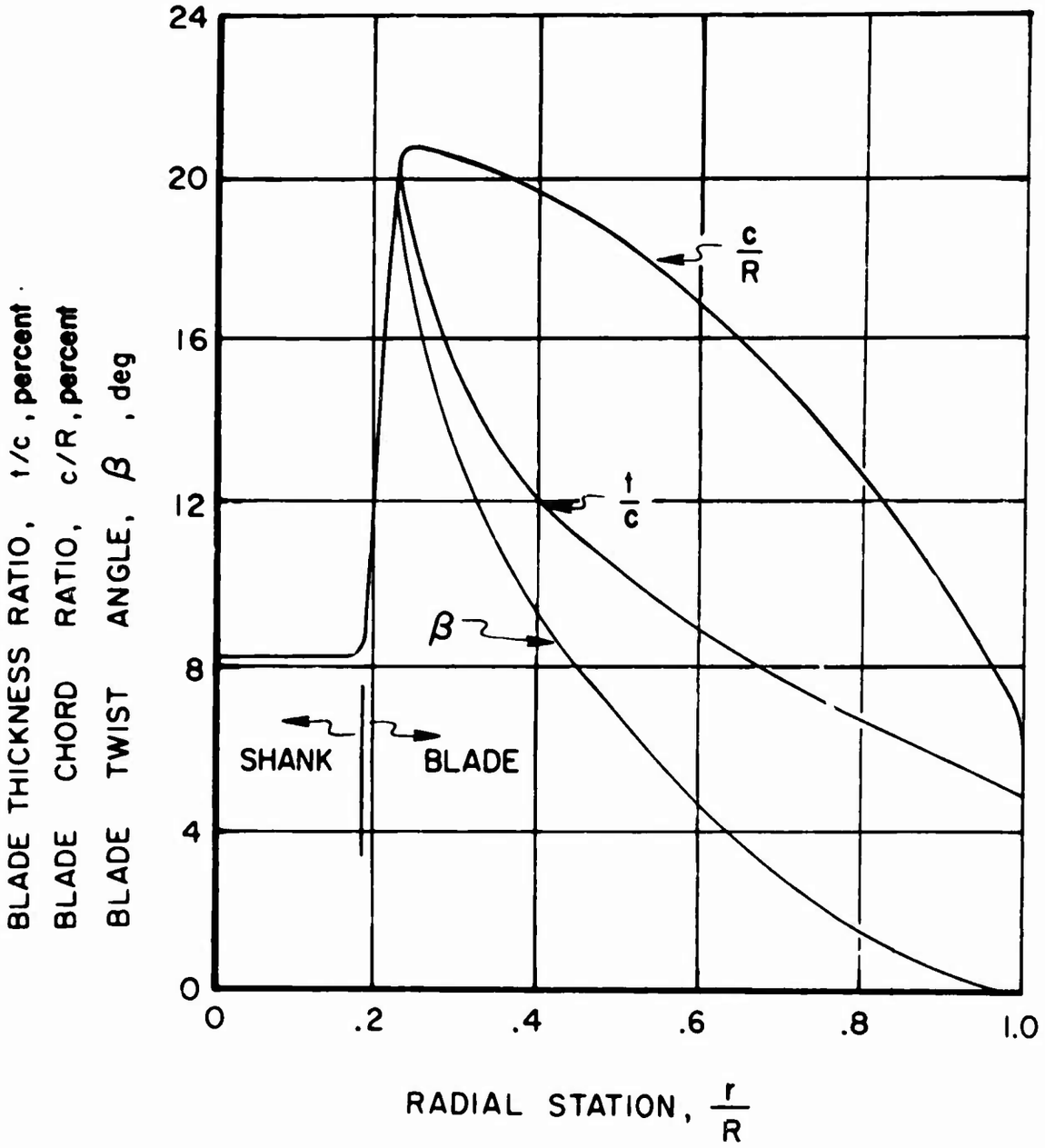

Figure 6. Model Propeller Blade Characteristics; Average of Right- and Left-Hand Four-Bladed Propellers.

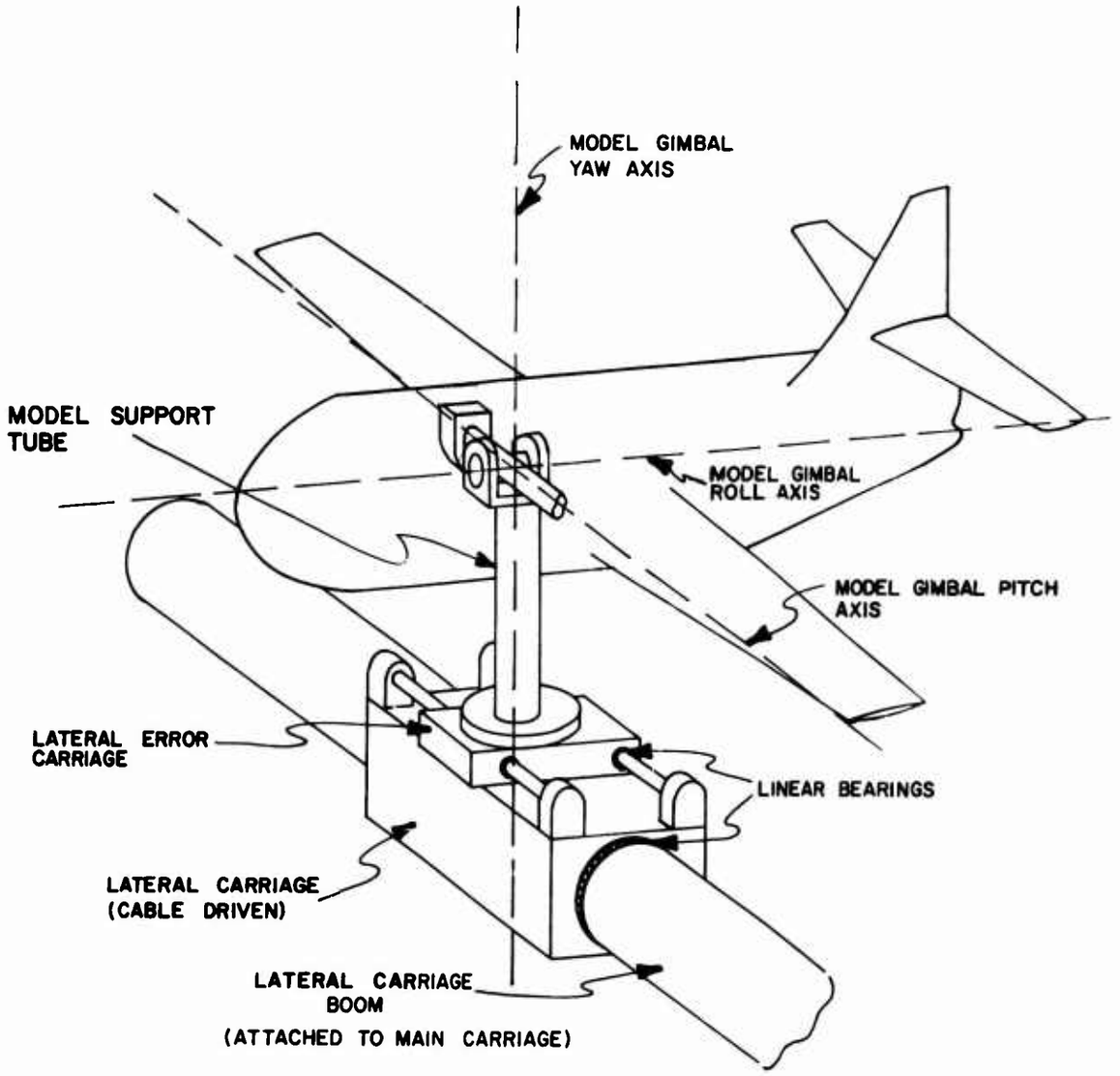

Figure 7. Schematic Representation of Lateral Carriage System, Model Support, and Gimbal Arrangement.

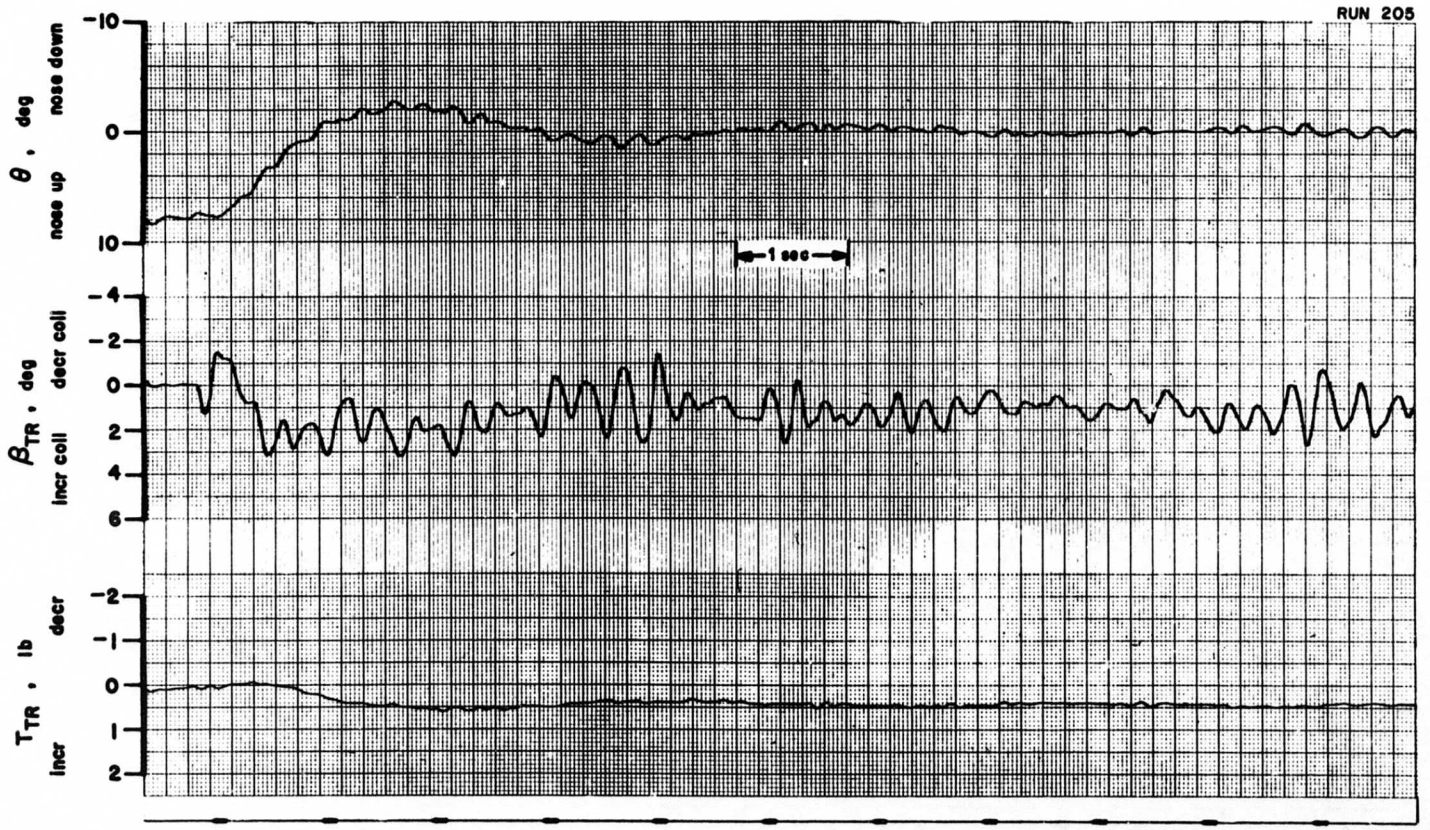

Figure 8. Typical Transient Response of Model Pitch Attitude Stabilization Feedback Loop.

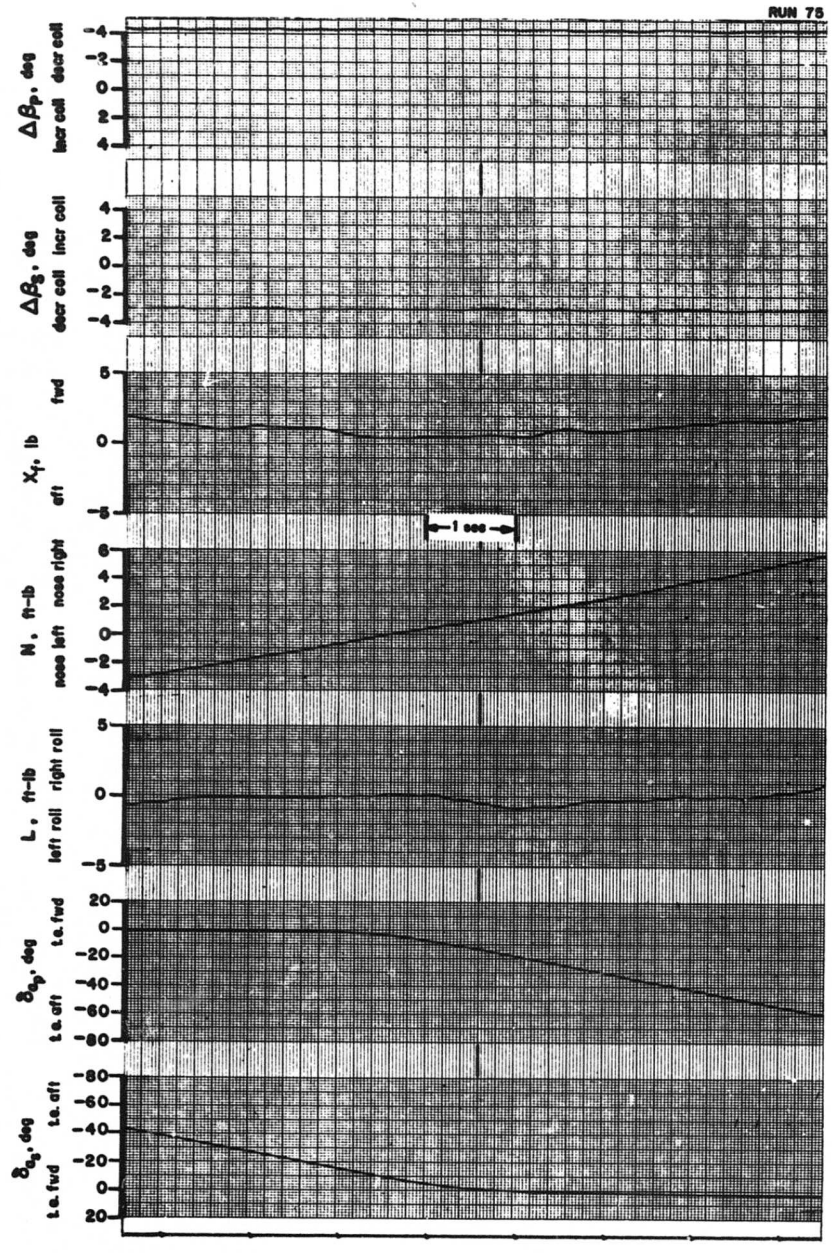

Figure 9. Static Test Data; Lateral/Directional Control Effectiveness. Aileron Effectiveness Only. No Differential Propeller Pitch Mixing.
$\theta = 0$, $\beta_{.75R} = 13.5^{\circ}$, and $U_f = 17.9$ ft/sec.
$i_w = 40^{\circ}$, $\delta_f = 60^{\circ}$, $i_t = 20^{\circ}$.

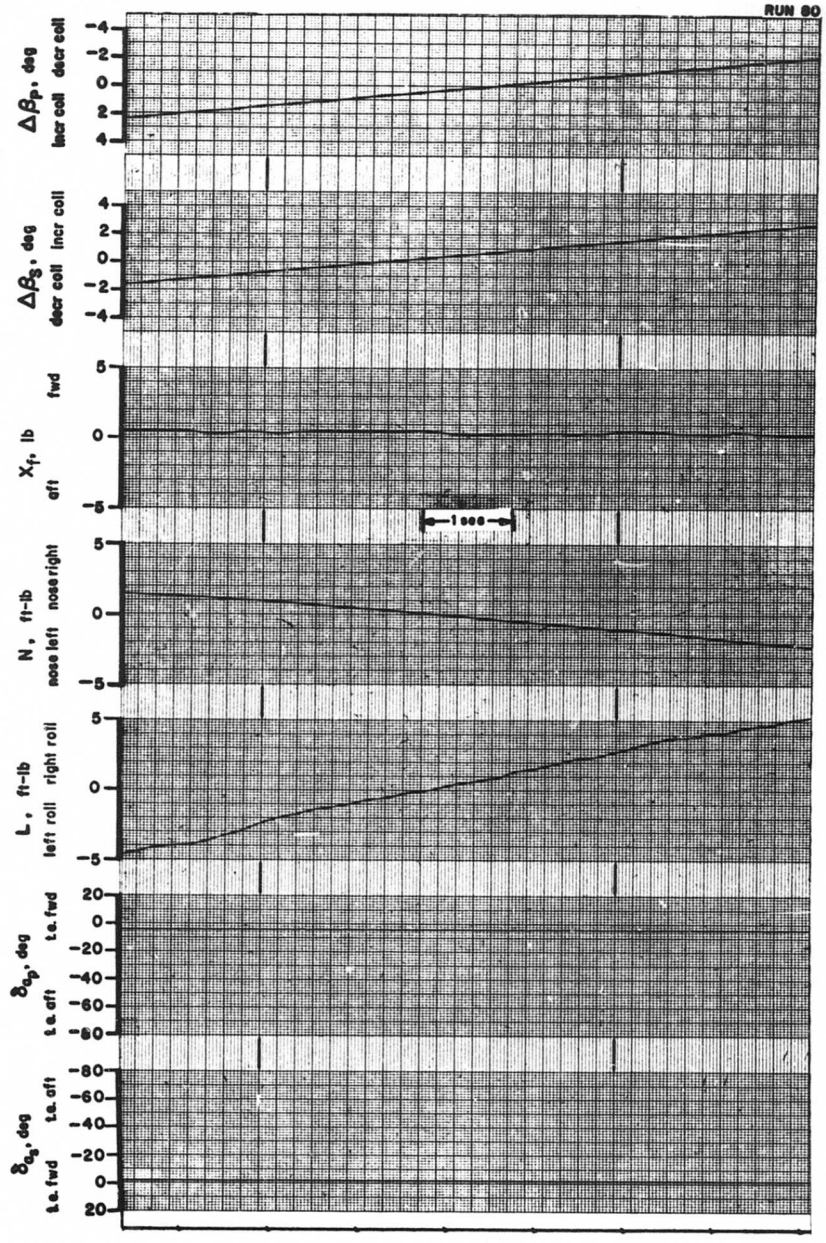

Figure 10. Static Test Data; Lateral/Directional Control Effectiveness. Differential Propeller Pitch Only. No Aileron Mixing. $\theta = 0$, $\beta_{.75R} = 13.5^{\circ}$, and $U_f = 17.9$ ft/sec.

$i_w = 40^{\circ}$, $\delta_f = 60^{\circ}$, $i_t = 20^{\circ}$.

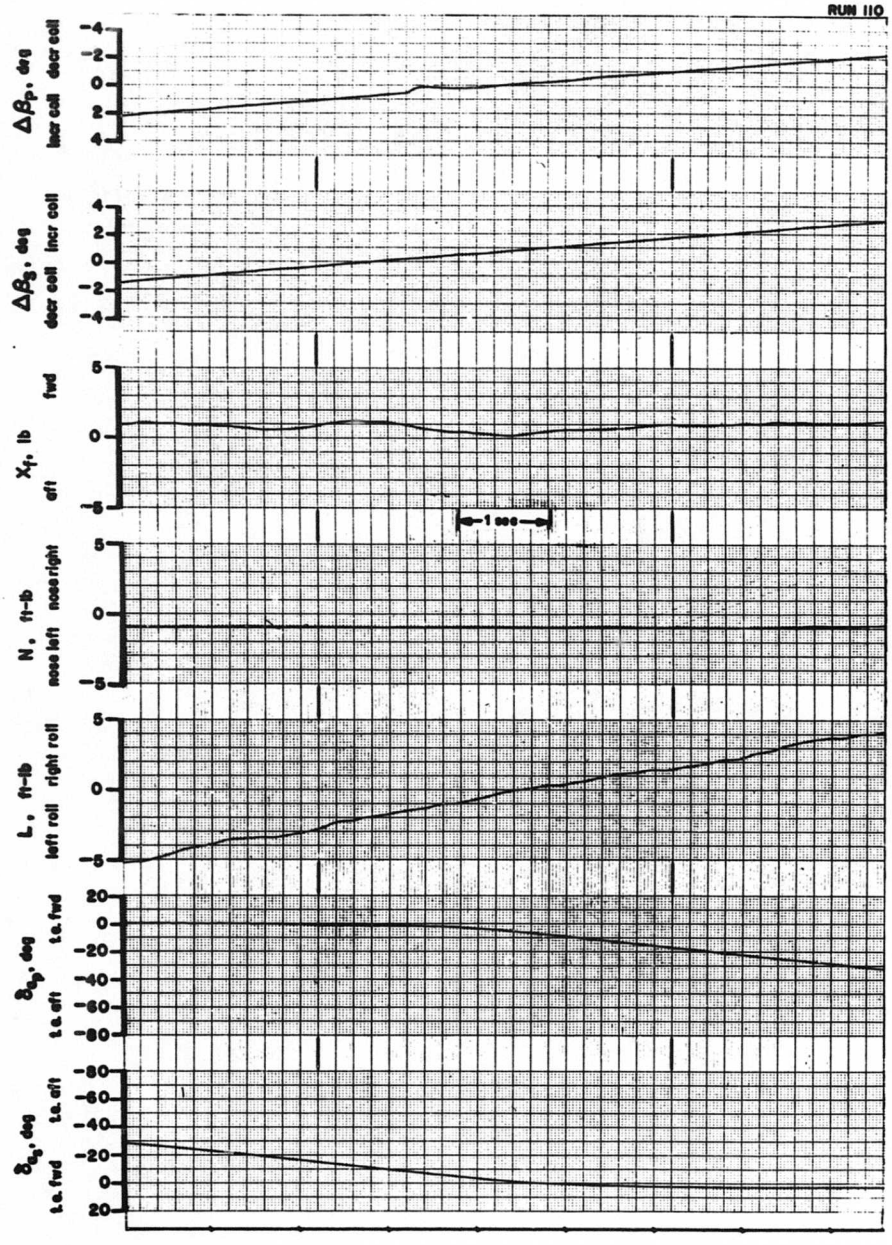

Figure 11. Static Test Data; Lateral/Directional Control Effectiveness. Aileron and Differential Propeller Pitch Mixed. $\theta = 0$, $\beta_{.75R} = 13.5°$, and $U_f = 17.9$ ft/sec. $i_w = 40°$, $\delta_f = 60°$, $i_t = 20°$.

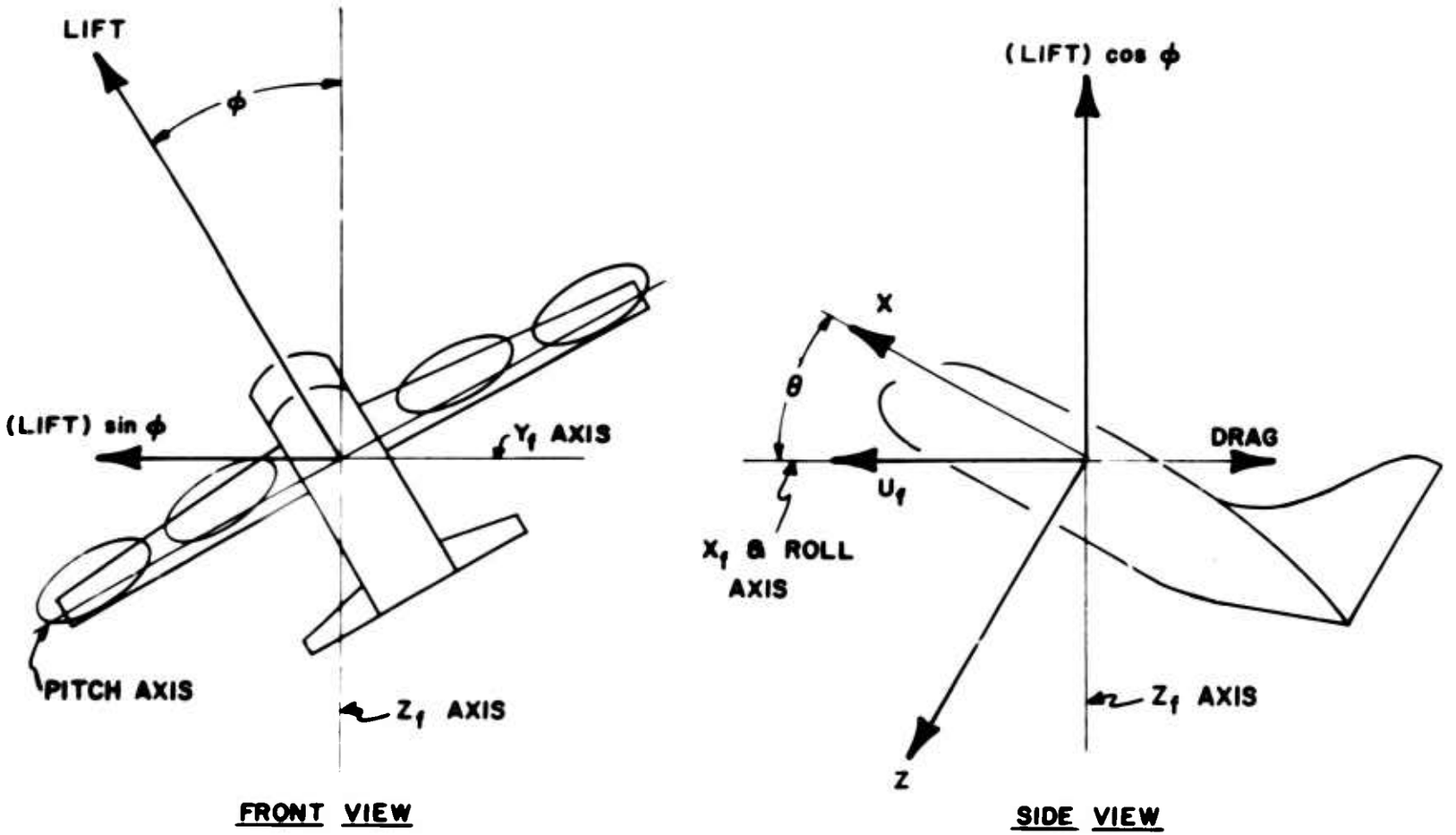

Figure 12. Diagram for Resolution of Model Forces From Static Test Data, ψ = 0.

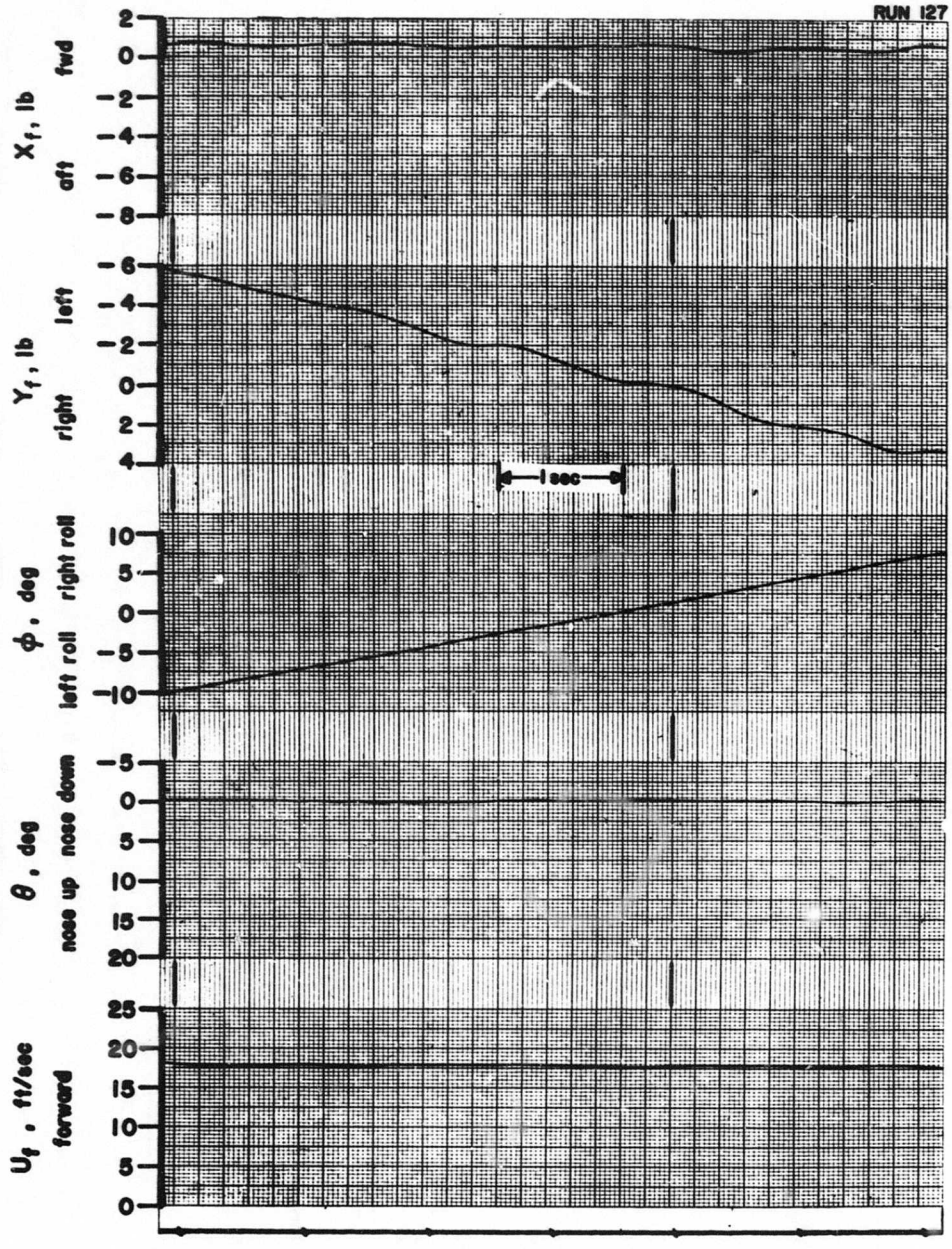

Figure 13. Static Test Data; Descent Condition Determination Ramp Input to Roll Attitude-Hold Loop.
$\beta_{.75R} = 13.5°$, $\delta_a = 0$, and $\Delta\beta = 0$.
$i_w = 40°$, $\delta_f = 60°$, $i_t = 20°$.

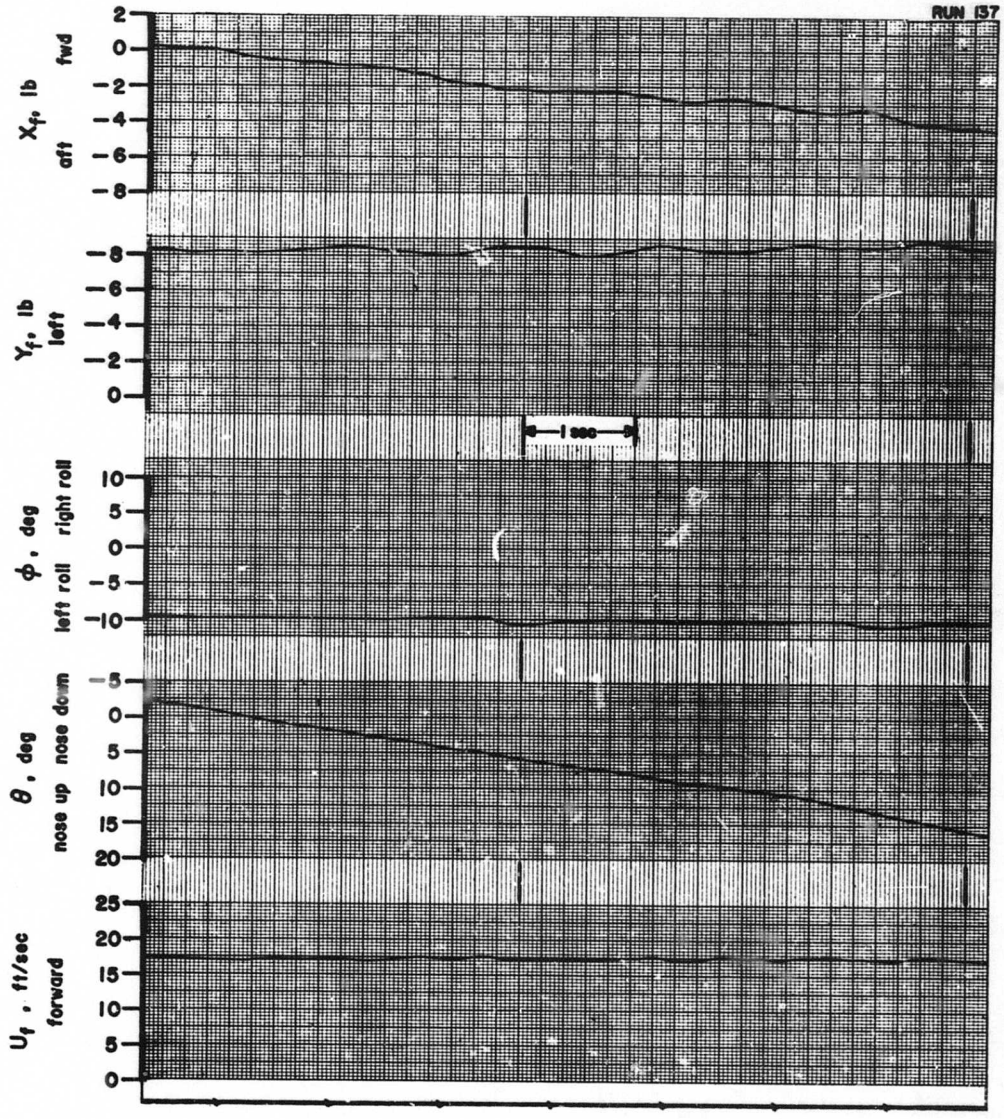

Figure 14. Static Test Data; Descent Condition Determination. Ramp Input to Pitch Attitude-Hold Loop.
$\beta_{.75R} = 13.5^\circ$, $\delta_a = 0$, and $\Delta\beta = 0$.
$i_w = 40^\circ$, $\delta_f = 60^\circ$, $i_t = 20^\circ$.

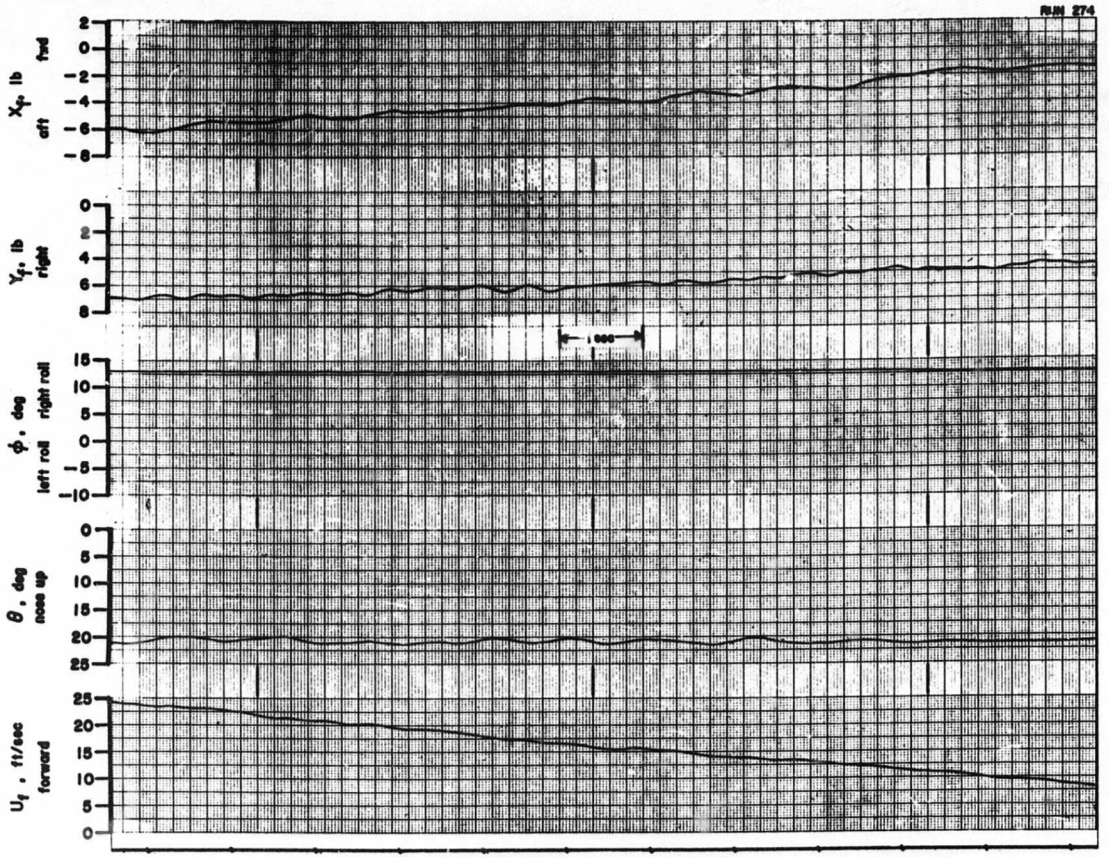

Figure 15. Static Test Data; Descent Condition Determination. Ramp Velocity Input.

$\beta_{.75R} = 11.5°$, $\delta_a = 0$, and $\Delta\beta = 0$.

$i_w = 40°$, $\delta_f = 60°$, $i_t = 20°$.

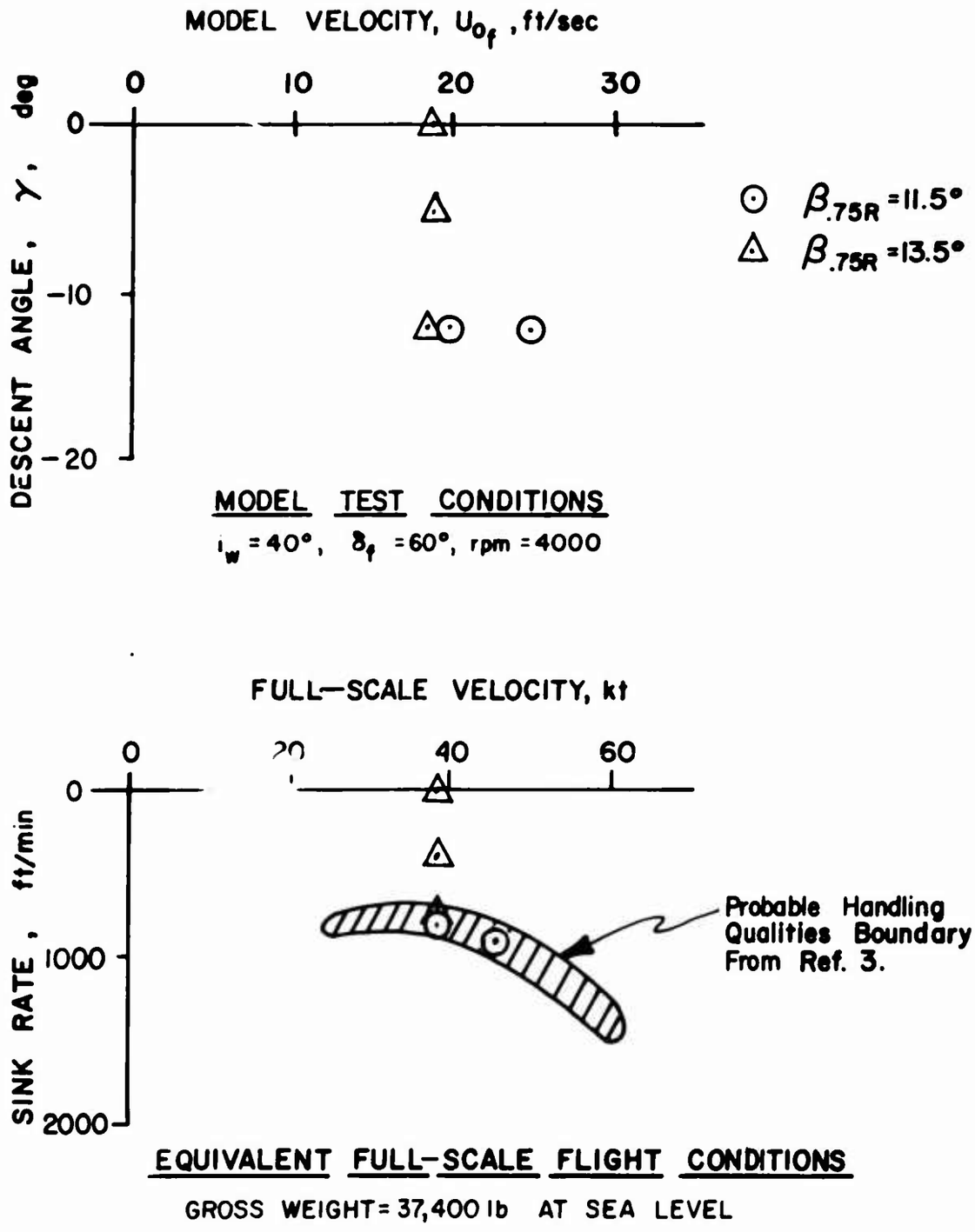

Figure 16. Summary of Descent Test Conditions, Model-Scale and Equivalent Full-Scale Flight Conditions.
$i_w = 40°$, $\delta_f = 60°$, $i_t = 20°$, for Model Tests.

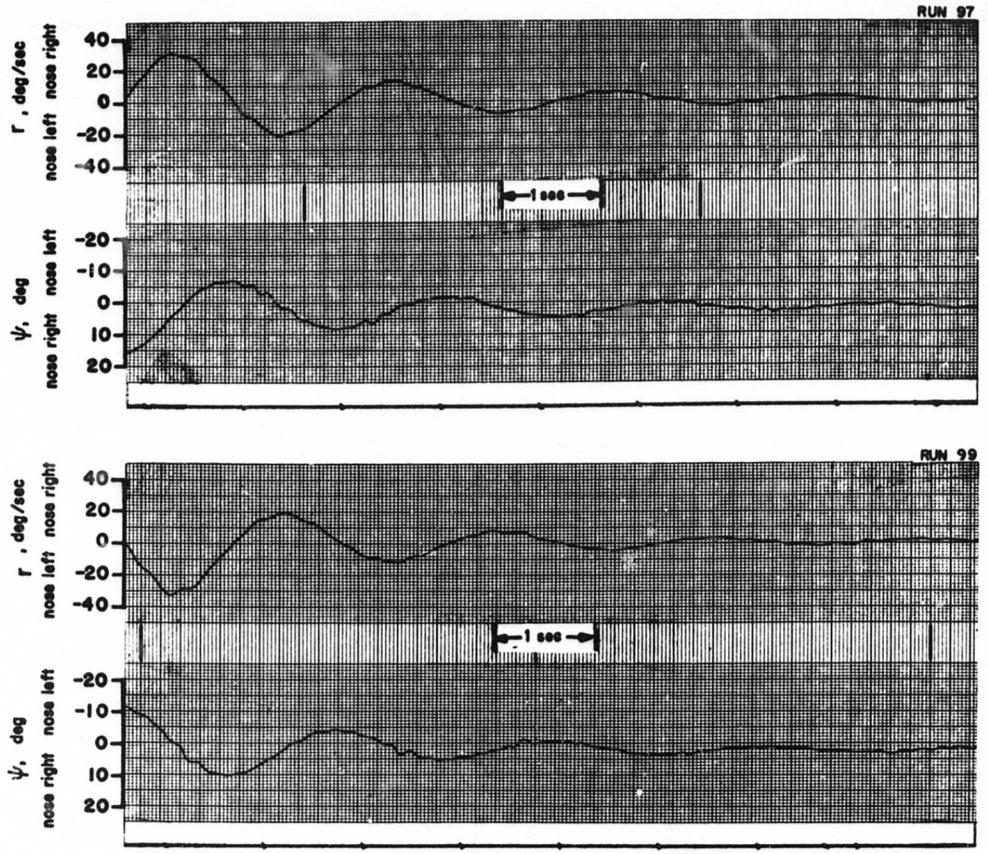

Figure 17. Dynamic Test Data; Directional Transient Response. One Degree of Freedom, ψ. $\theta = 0$, $\beta_{.75R} = 11.5^{o}$, $\gamma = 0$, and $U_f = 17.4$ ft/sec. $i_w = 40^{o}$, $\delta_f = 60^{o}$, $i_t = 20^{o}$.

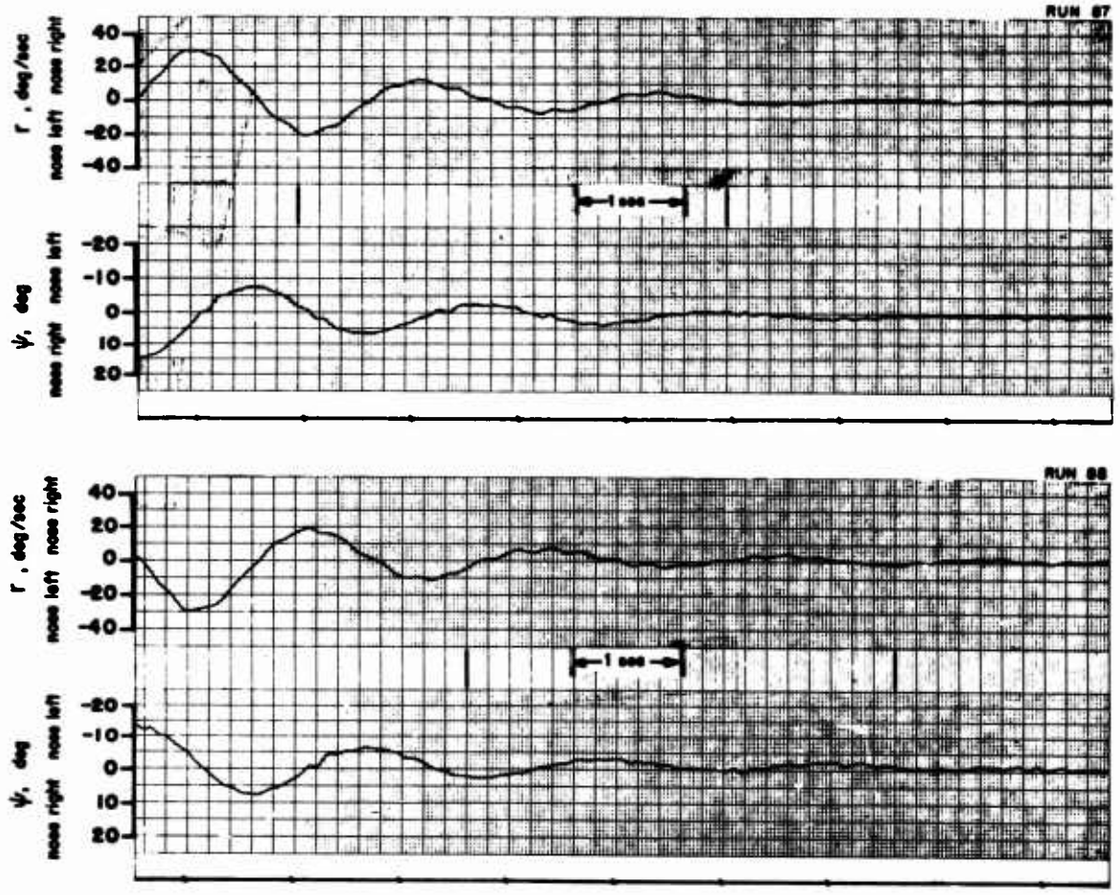

Figure 18. Dynamic Test Data; Directional Transient Response. One Degree of Freedom, Ψ.
$\theta = 0$, $\beta_{.75R} = 13.5°$, $\gamma = 0$, and $U_f = 17.8$ ft/sec.
$i_w = 40°$, $\delta_f = 60°$, $i_t = 20°$.

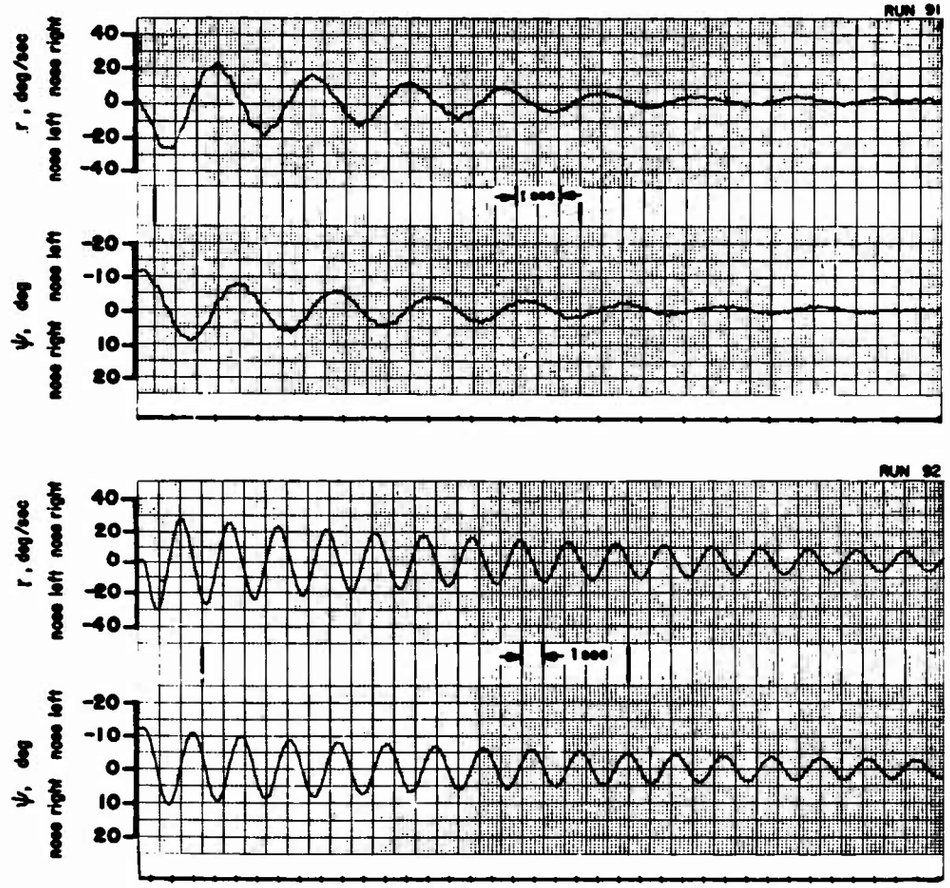

Figure 19. Dynamic Test Data; Directional Transient Response. One Degree of Freedom, Ψ. $\theta = 0$, $\beta_{.75R} = 13.5°$, $\gamma = 0$, and $U_f = 0$ ft/sec. $i_w = 40°$, $\delta_f = 60°$, $i_t = 20°$.

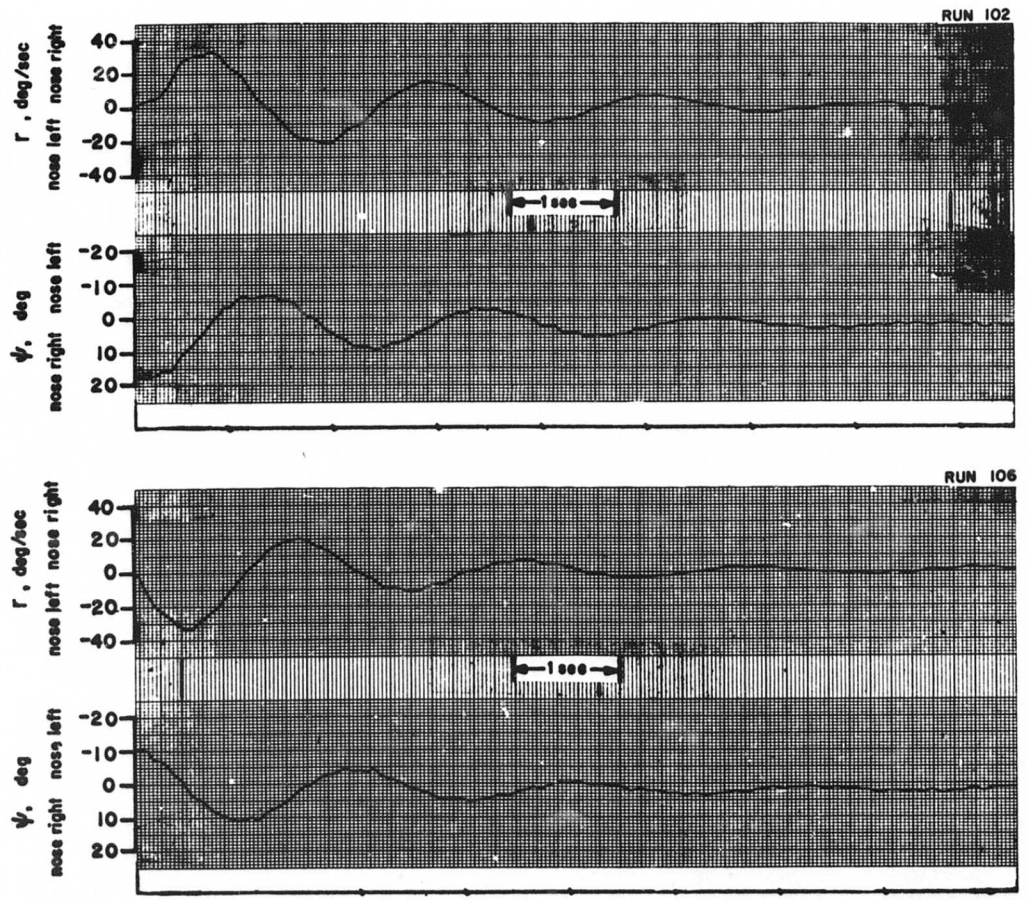

Figure 20. Dynamic Test Data; Directional Transient Response. One Degree of Freedom, Ψ. $\theta = 0$, $\beta_{.75R} = 13.5°$, $\gamma = 0$, and $U_f = 19.4$ ft/sec. $i_w = 40°$, $\delta_f = 60°$, $i_t = 20°$.

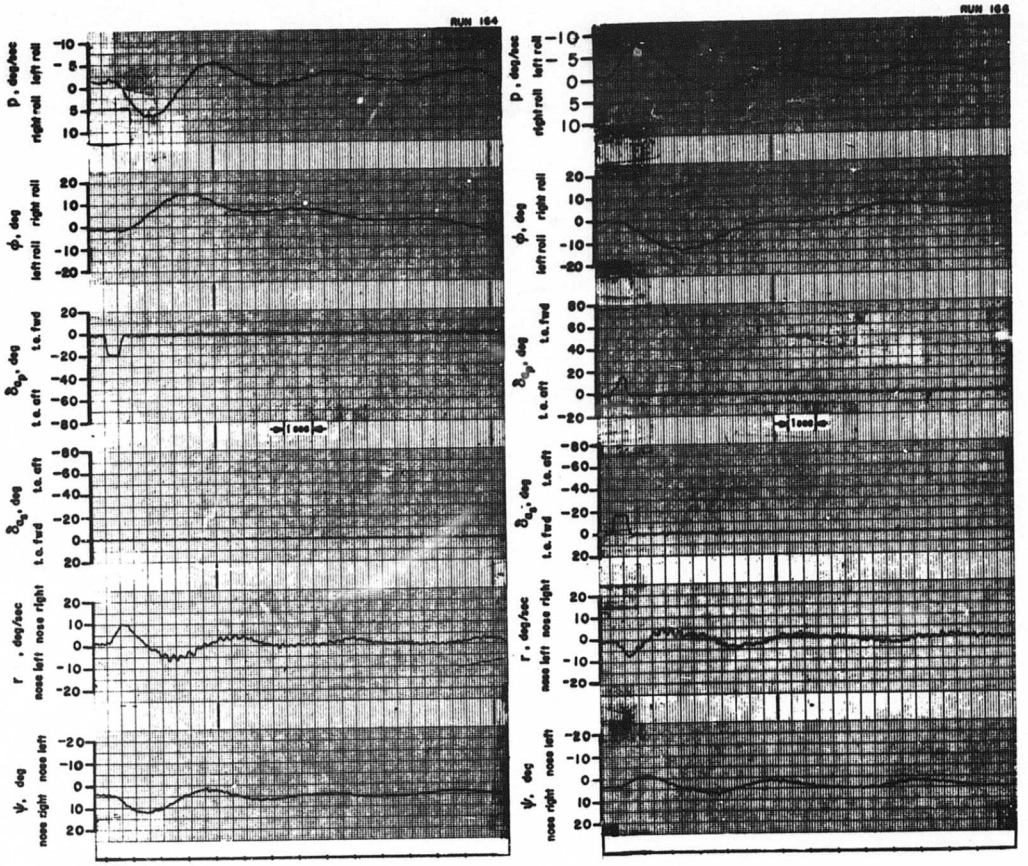

Figure 21. Dynamic Test Data; Lateral/Directional Transient Response. Two Degrees of Freedom, ϕ-Ψ.
$\theta = 0$, $\beta_{.75R} = 13.5°$, $\gamma = 0$, and $U_f = 17.6$ ft/sec.
$i_w = 40°$, $\delta_f = 60°$, $i_t = 20°$.

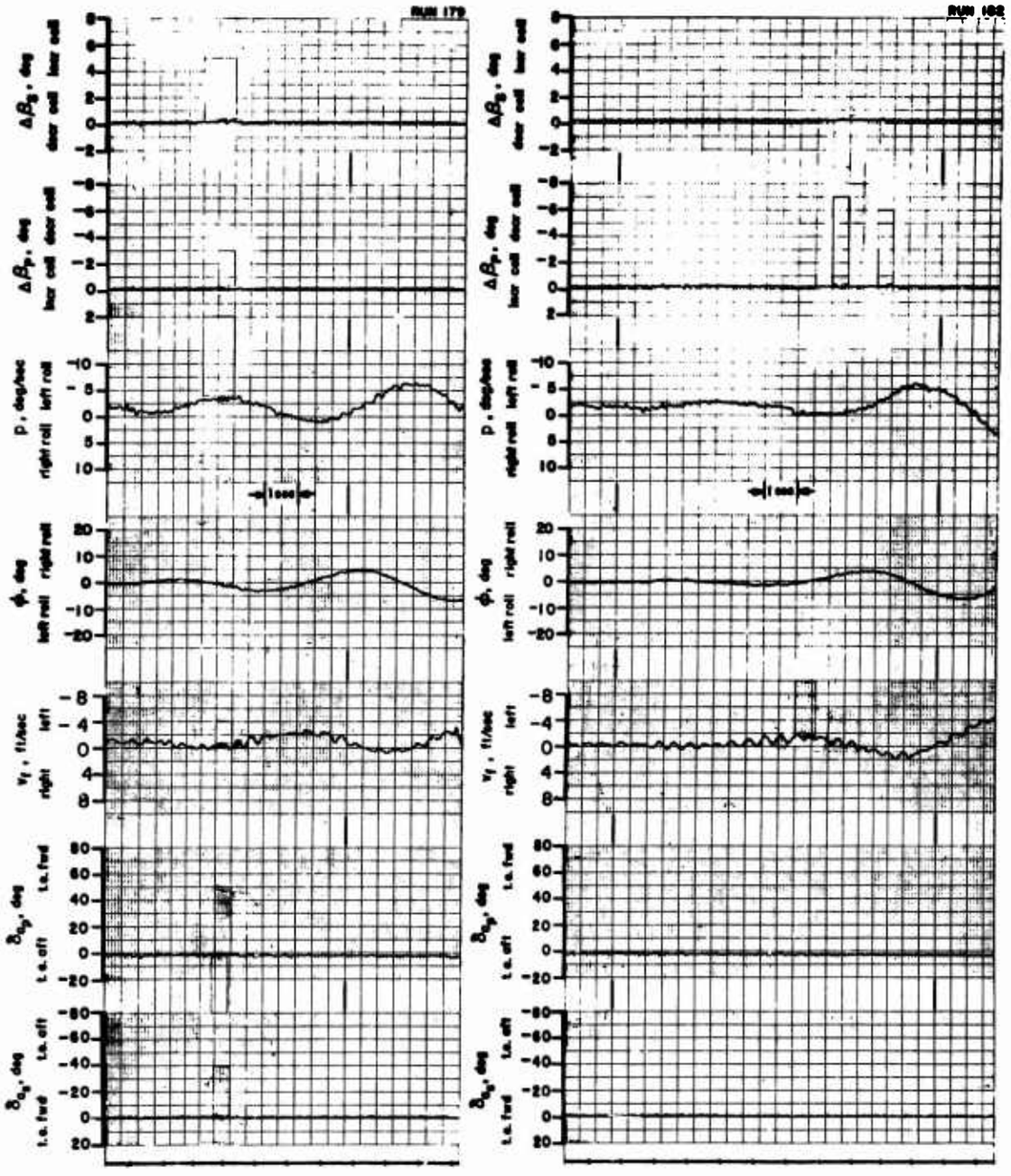

Figure 22. Dynamic Test Data; Lateral/Directional Transient Response. Two Degrees of Freedom, ϕ-v_f.

$\theta = 0$, $\beta_{.75R} = 13.5°$, $\gamma = 0$, and $U_f = 18.4$ ft/sec.

$i_w = 40°$, $\delta_f = 60°$, $i_t = 20°$.

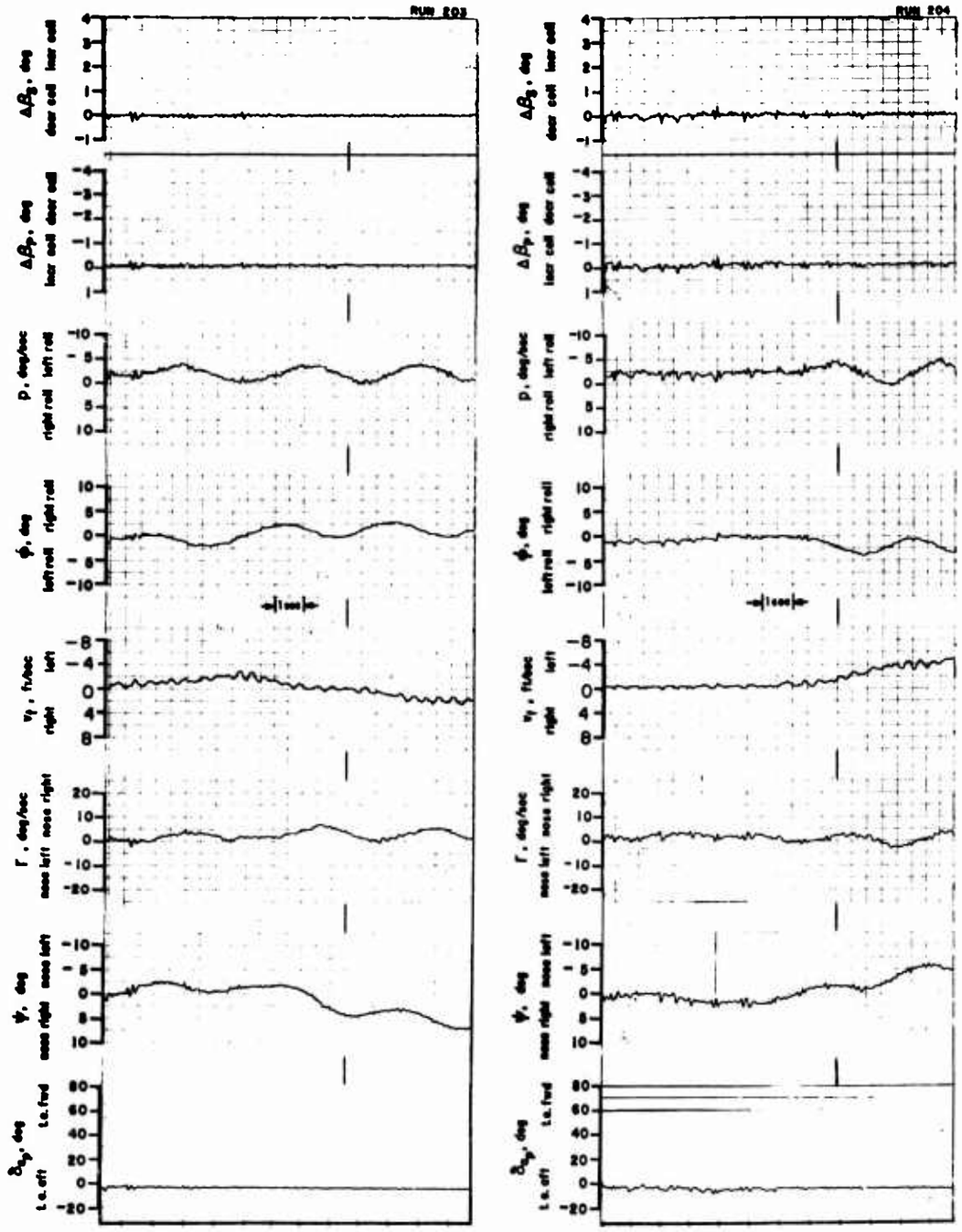

Figure 23. Dynamic Test Data; Lateral/Directional Transient Response. Three Degrees of Freedom, ϕ-Ψ-v_f.

$\theta = 0$, $\beta_{.75R} = 13.5°$, $\gamma = 0$, and $U_f = 17.9$ ft/sec.

$i_w = 40°$, $\delta_f = 60°$, $i_t = 20°$.

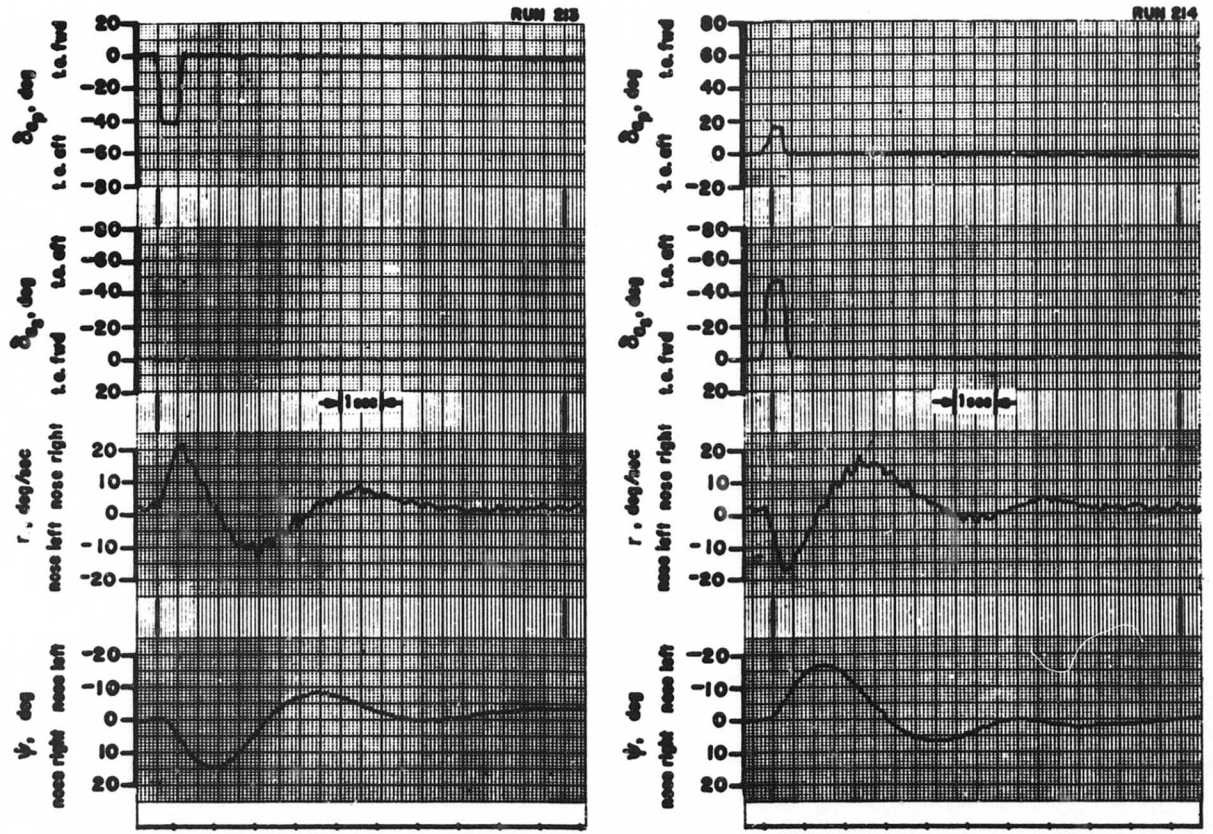

Figure 24. Dynamic Test Data; Lateral/Directional Transient Response. One Degree of Freedom, Ψ.
$\theta = 10°$, $\beta_{.75R} = 13.5°$, $\gamma = -5°$, and $U_f = 17.8$ ft/sec.
$i_w = 40°$, $\delta_f = 60°$, $i_t = 20°$.

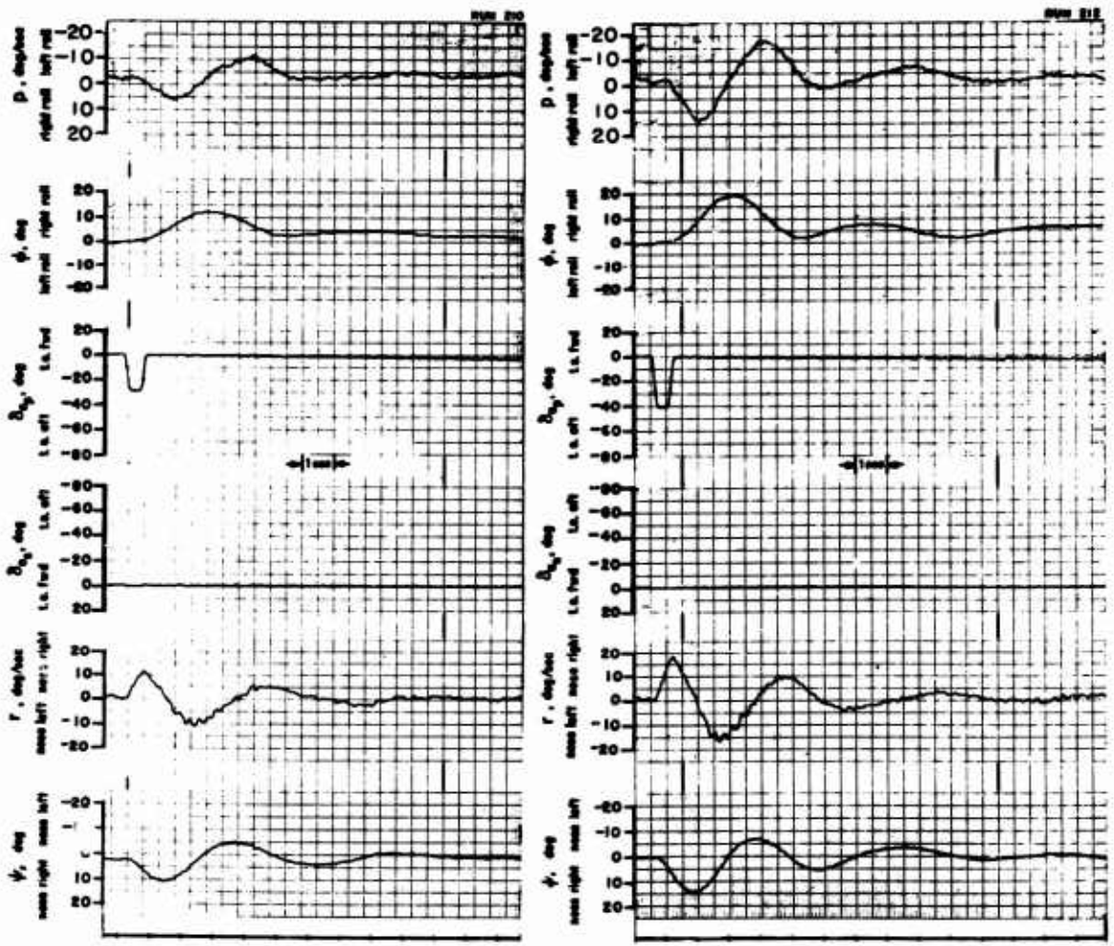

Figure 25. Dynamic Test Data; Lateral/Directional Transient Response. Two Degrees of Freedom, ϕ-Ψ. $\theta = 10^{\circ}$, $\beta_{.75R} = 13.5^{\circ}$, $\gamma = -5^{\circ}$, and $U_f = 17.7$ ft/sec. $i_w = 40^{\circ}$, $\delta_f = 60^{\circ}$, $i_t = 20^{\circ}$.

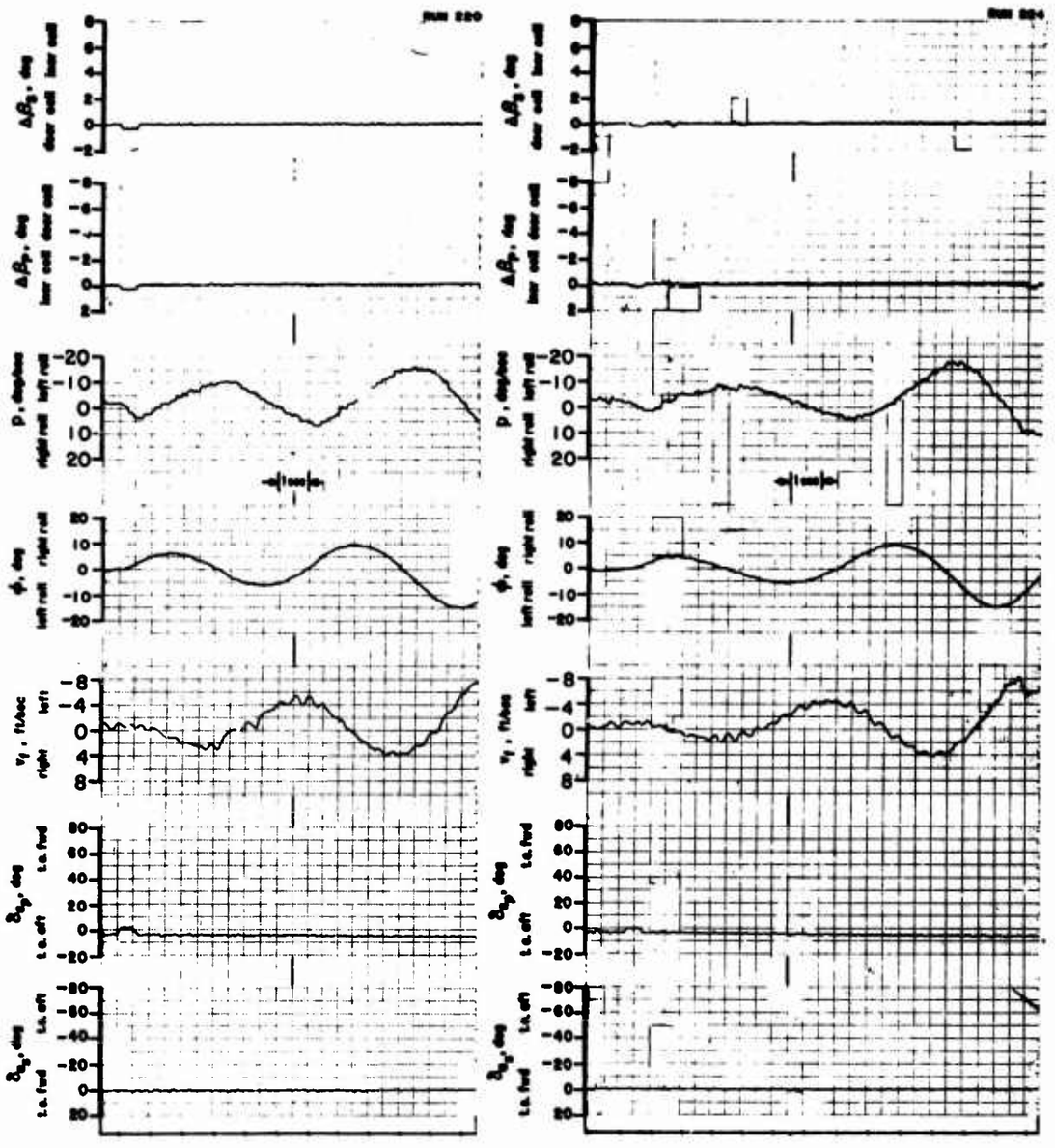

Figure 26. Dynamic Test Data; Lateral/Directional Transient Response. Two Degrees of Freedom, ϕ-v.
$\theta = 10^{o}$, $\beta_{.75R} = 13.5^{o}$, $\gamma = -5^{o}$, and $U_f = 17.6$ ft/sec.
$i_w = 40^{o}$, $\delta_f = 60^{o}$, $i_t = 20^{o}$.

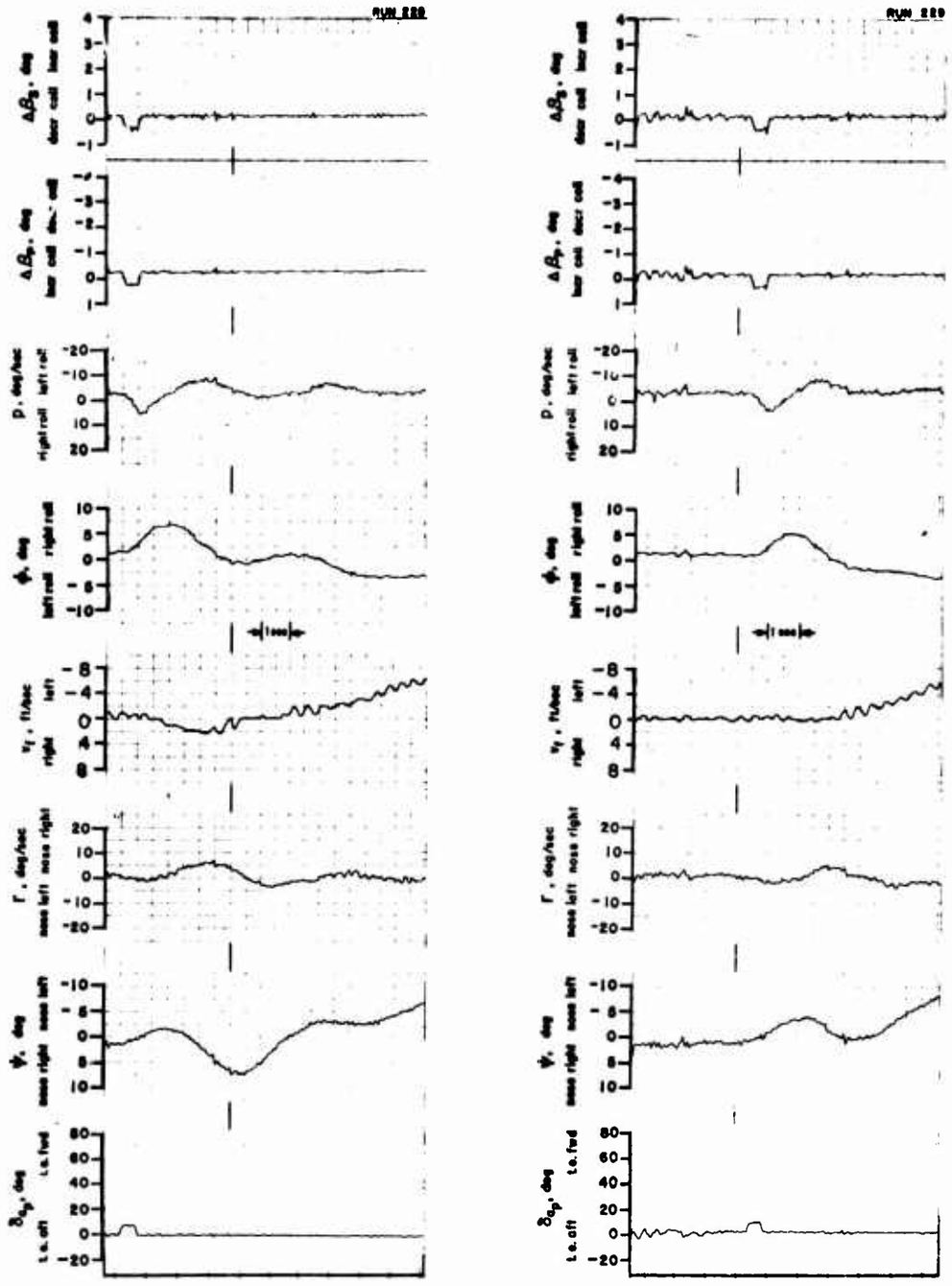

Figure 27. Dynamic Test Data; Lateral/Directional Transient Response. Three Degrees of Freedom, ϕ-Ψ-v_f.
$\theta = 10^o$, $\beta_{.75R} = 13.5^o$, $\gamma = -5^o$, and $U_f = 18.4$ ft/sec.
$i_w = 40^o$, $\delta_f = 60^o$, $i_t = 20^o$.

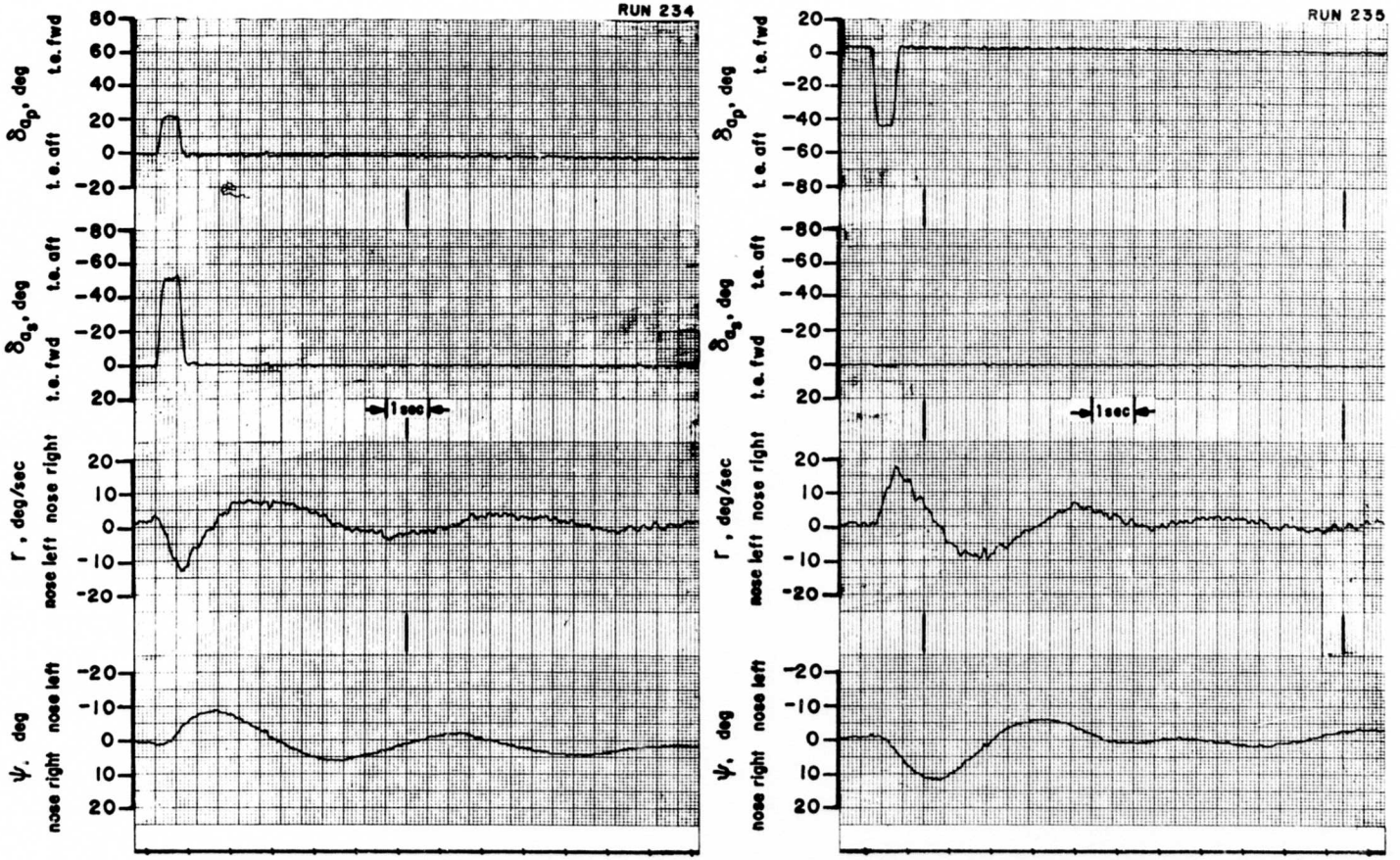

Figure 28. Dynamic Test Data; Lateral/Directional Transient Response. One Degree of Freedom, ψ. $\theta = 20°$, $\beta_{.75R} = 13.5°$, $\gamma = -11°$, and $U_f = 18.6$ ft/sec. $i_w = 40°$, $\delta_f = 60°$, $i_t = 20°$.

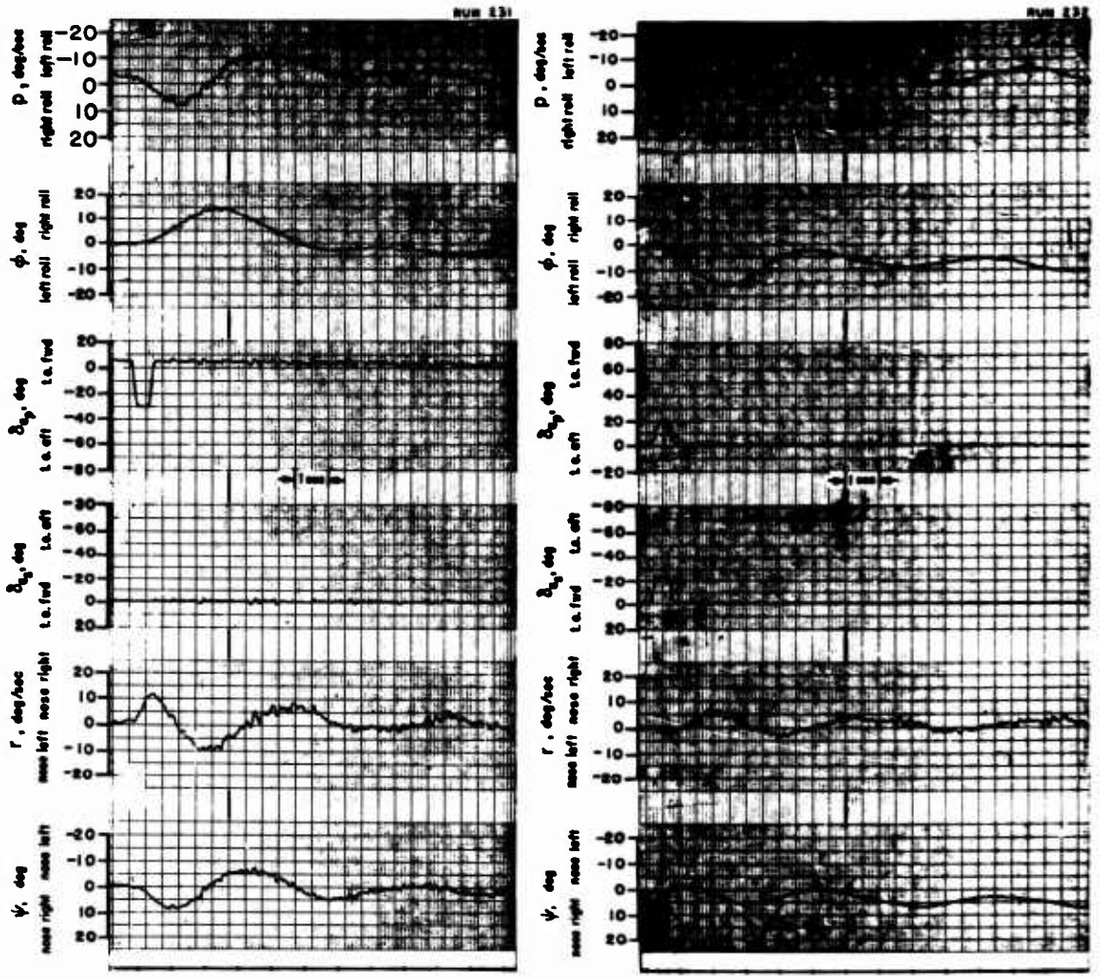

Figure 29. Dynamic Test Data; Lateral/Directional Transient Response. Two Degrees of Freedom, ϕ-ψ. $\theta = 20^{\circ}$, $\theta_{.75R} = 13.5^{\circ}$, $\gamma = -11^{\circ}$, and $U_f = 18.6$ ft/sec. $i_w = 40^{\circ}$, $\delta_f = 60^{\circ}$, $i_t = 20^{\circ}$.

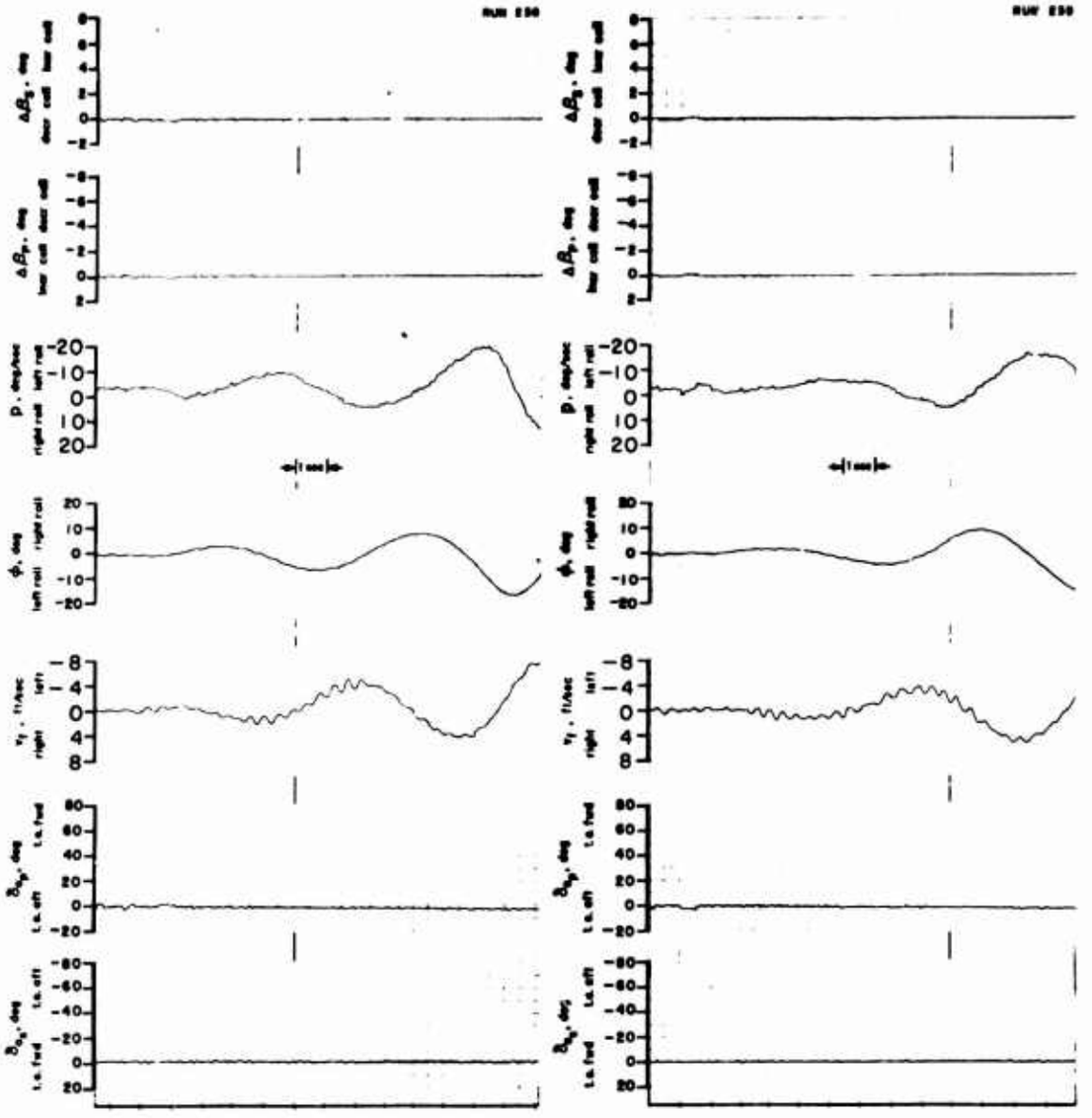

Figure 30. Dynamic Test Data; Lateral/Directional Transient Response. Two Degrees of Freedom, ϕ-v_f.

$\theta = 20^o$, $\beta_{.75R} = 13.5^o$, $\gamma = -11^o$, and $U_f = 18.4$ ft/sec.

$i_w = 40^o$, $\delta_f = 60^o$, $i_t = 20^o$.

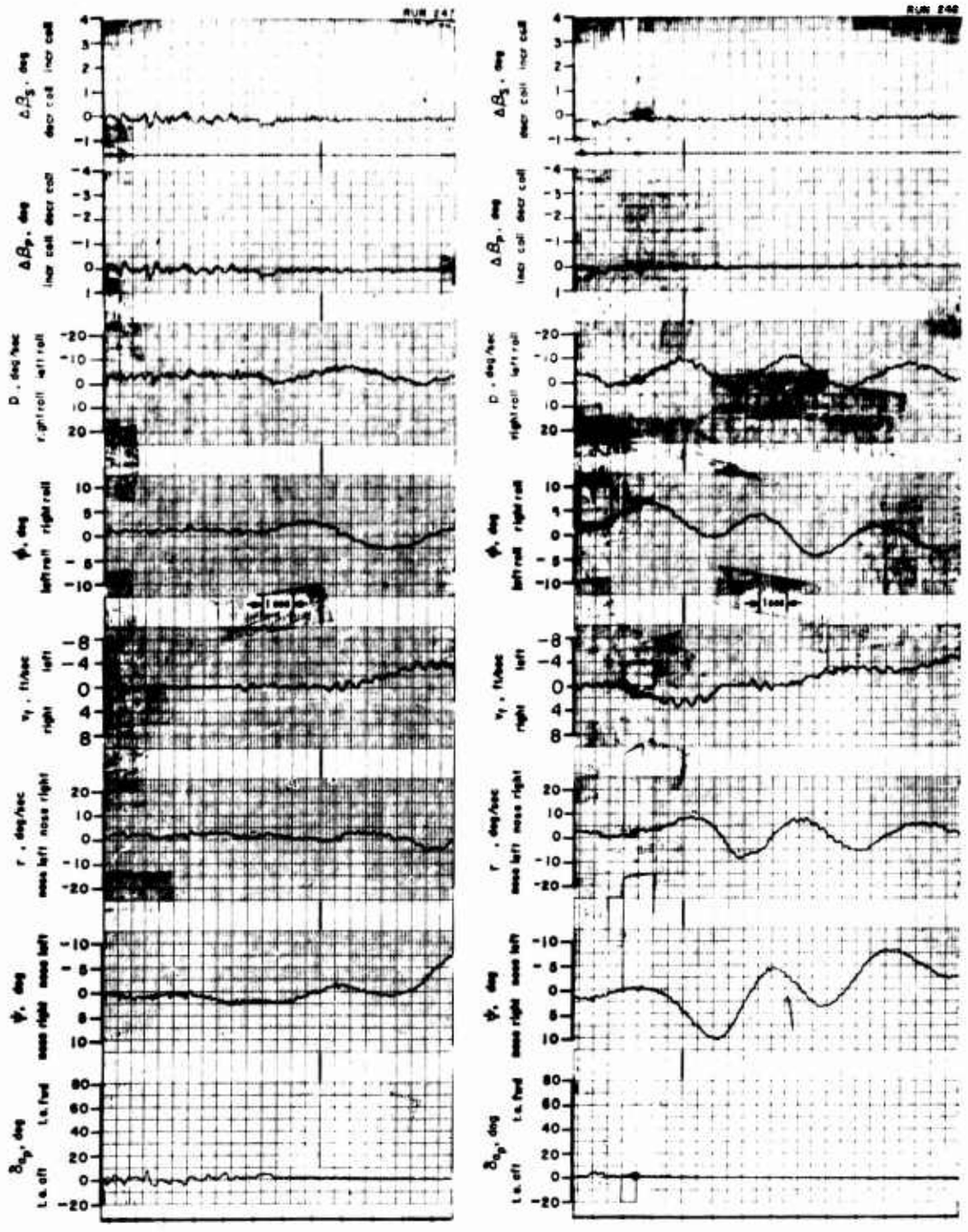

Figure 31. Dynamic Test Data; Lateral/Directional Transient Response. Three Degrees of Freedom, ϕ-Ψ-v_f.

$\theta = 20°$, $\beta_{.75R} = 13.5°$, $\gamma = -11°$, and $U_f = 18.4$ ft/sec.

$i_w = 40°$, $\delta_f = 60°$, $i_t = 20°$.

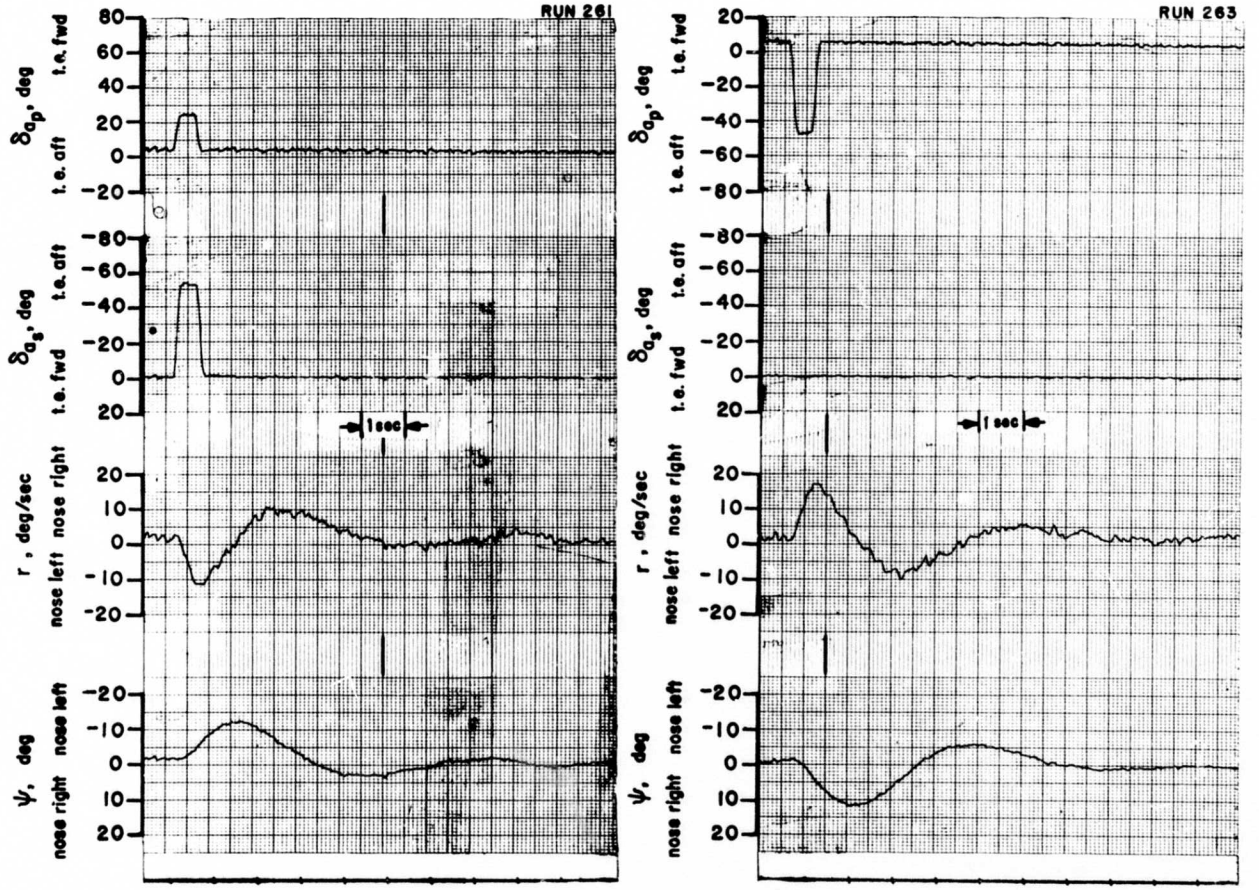

Figure 32. Dynamic Test Data; Lateral/Directional Transient Response. One Degree of Freedom, Ψ. $\theta = 20^{\circ}$, $\beta_{.75R} = 11.5^{\circ}$, $\gamma = -11^{\circ}$, and $U_f = 18.1$ ft/sec. $i_w = 40^{\circ}$, $\delta_f = 60^{\circ}$, $i_t = 20^{\circ}$.

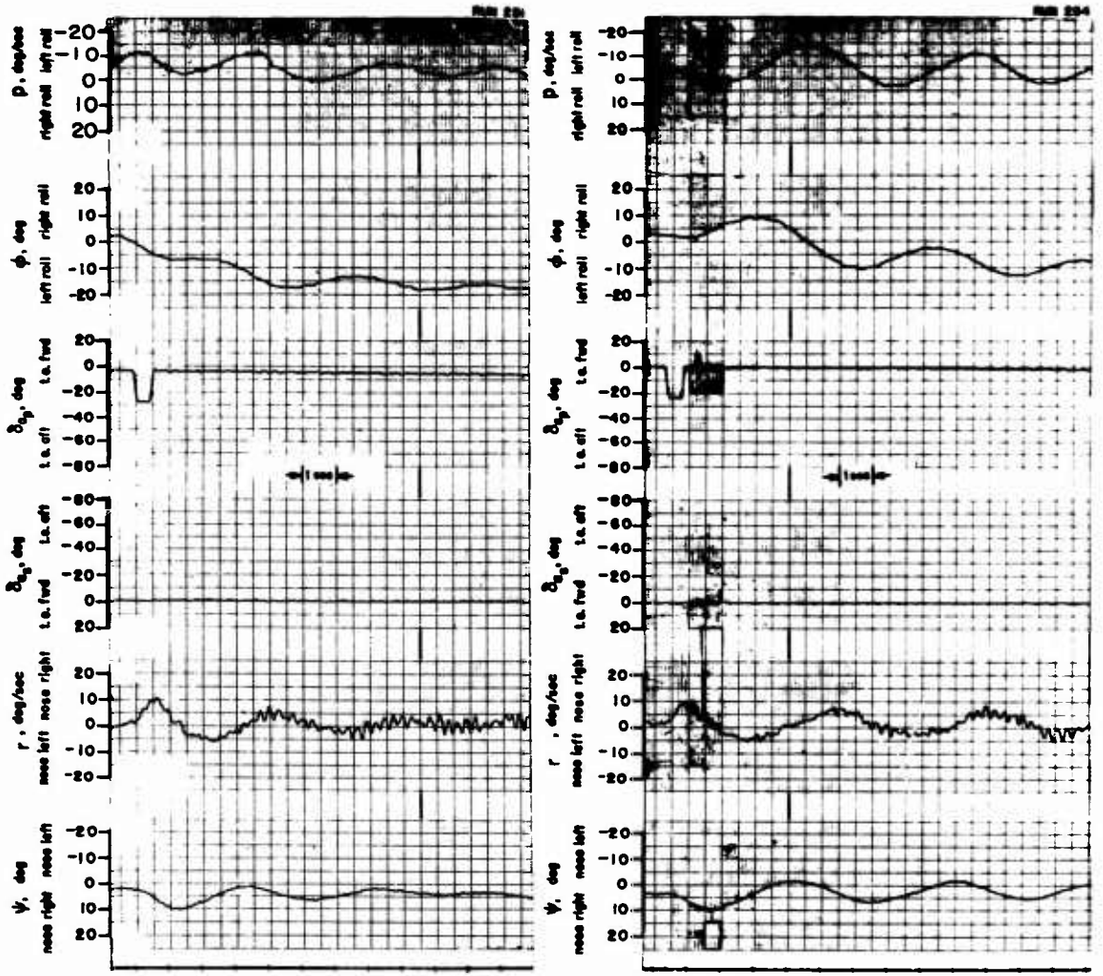

Figure 33. Dynamic Test Data; Lateral/Directional Transient Response. Two Degrees of Freedom, ϕ-Ψ. $\theta = 20°$, $\theta_{.75R} = 11.5°$, $\gamma = -11°$, and $U_f = 18.8$ ft/sec. $i_w = 40°$, $\delta_f = 60°$, $i_t = 20°$.

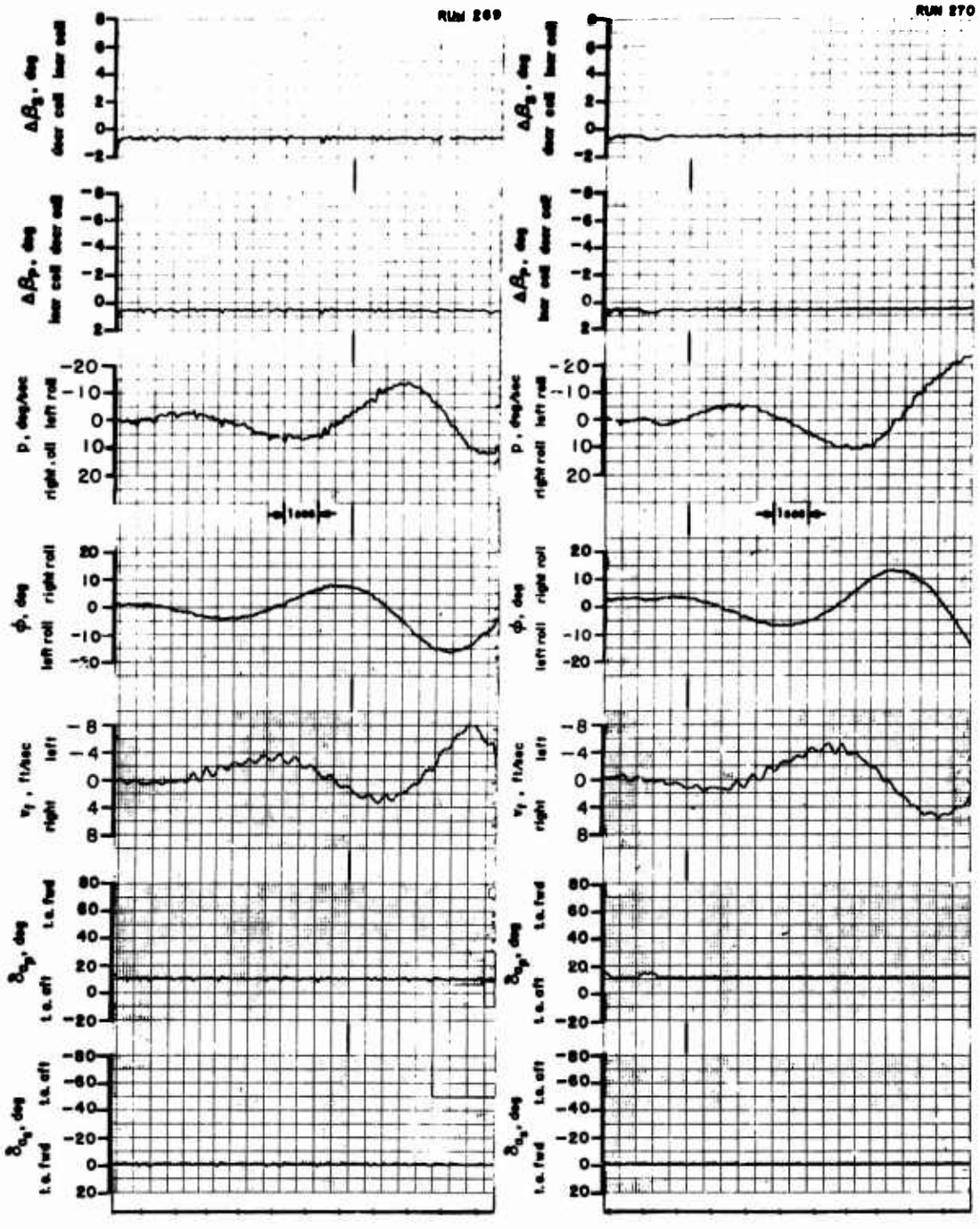

Figure 34. Dynamic Test Data; Lateral/Directional Transient Response. Two Degrees of Freedom, ϕ-v_f.
$\theta = 20°$, $\beta_{.75R} = 11.5°$, $\gamma = -11°$, and $U_f = 18.4$ ft/sec.
$i_w = 40°$, $\delta_f = 60°$, $i_t = 20°$.

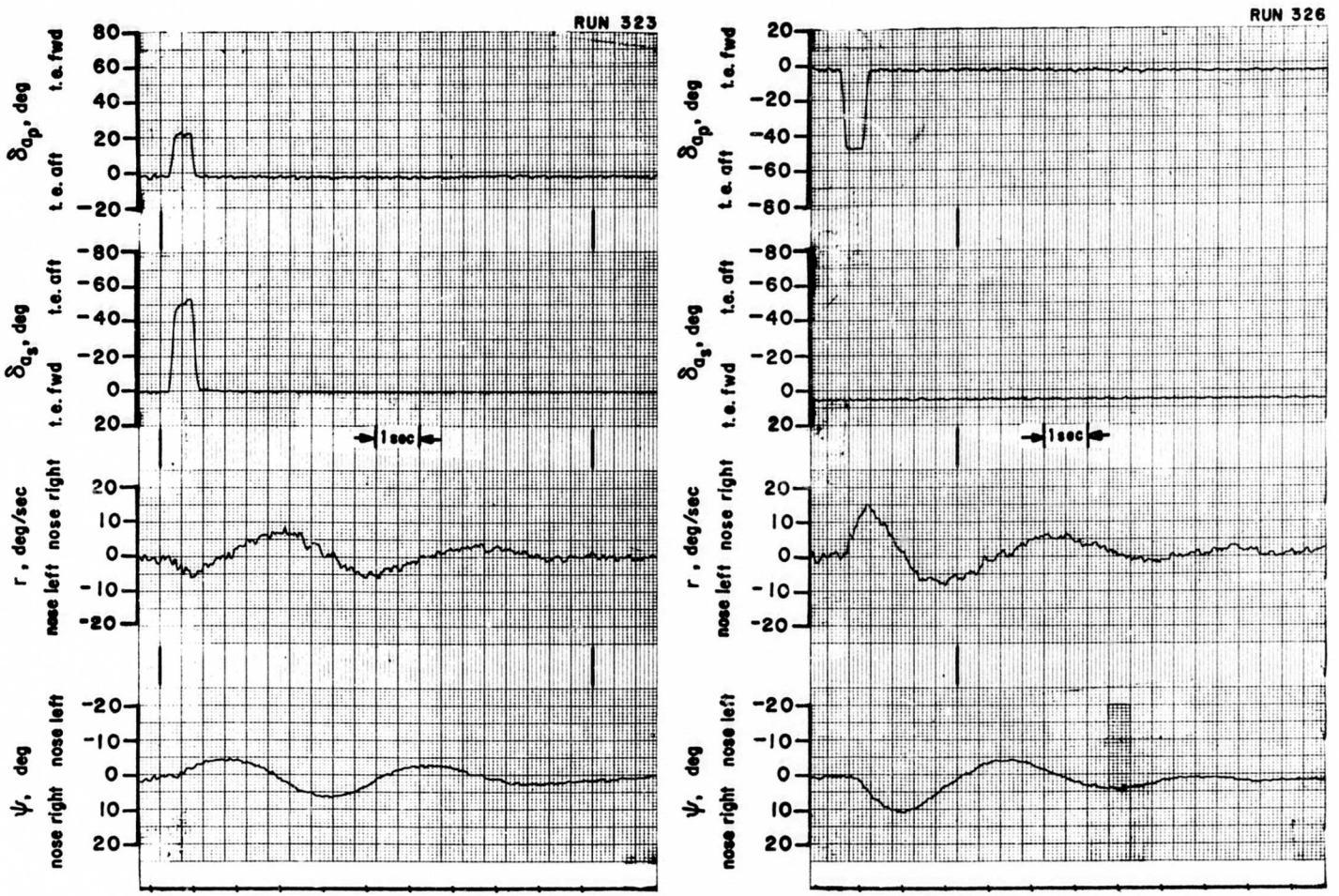

Figure 35. Dynamic Test Data; Lateral/Directional Transient Response. One Degree of Freedom, Y. $\theta = 20°$, $\beta_{.75R} = 11.5°$, $\gamma = -11°$, and $U_f = 23.5$ ft/sec. $i_w = 40°$, $\delta_f = 60°$, $i_t = 20°$.

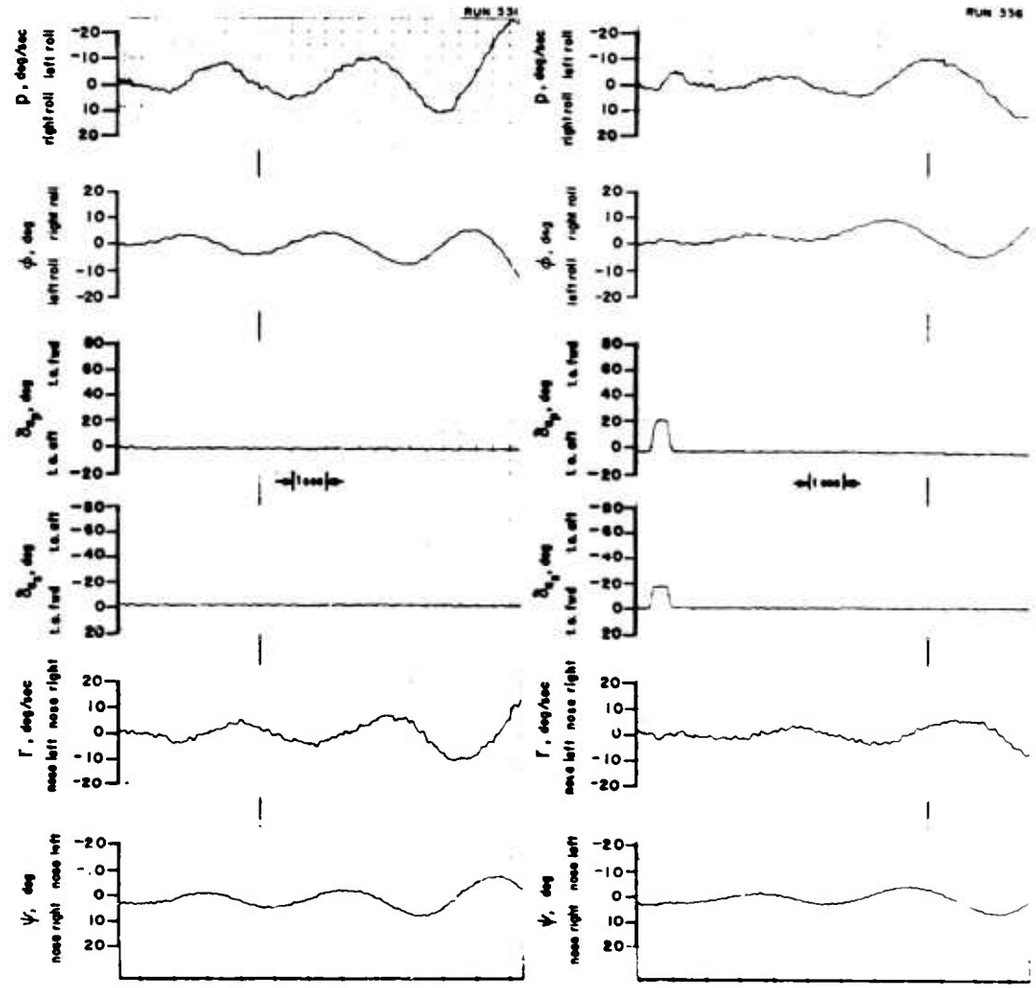

Figure 36. Dynamic Test Data; Lateral/Directional Transient Response. Two Degrees of Freedom, β-γ. $\theta = 20°$, $\theta_{.75R} = 11.5°$, $\gamma = -11°$, and $U_f = 24$ ft/sec. $i_w = 40°$, $\epsilon_f = 60°$, $i_t = 20°$.

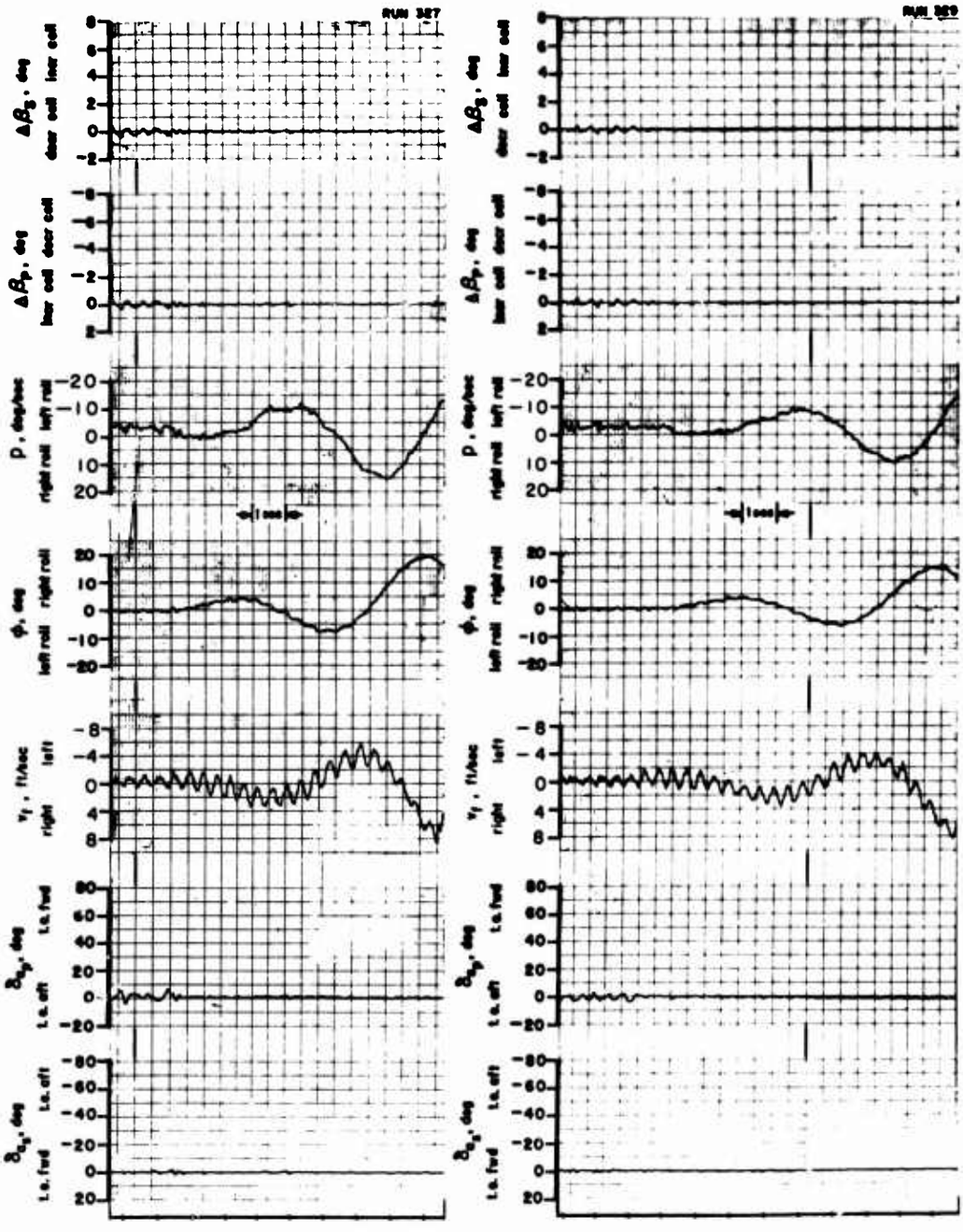

Figure 37. Dynamic Test Data; Lateral/Directional Transient Response. Two Degrees of Freedom, ϕ-v_f.
$\theta = 20^\circ$, $\beta_{.75R} = 11.5^\circ$, $\gamma = -11^\circ$, and $U_f = 23.6$ ft/sec.
$i_w = 40^\circ$, $\delta_f = 60^\circ$, $i_t = 20^\circ$.

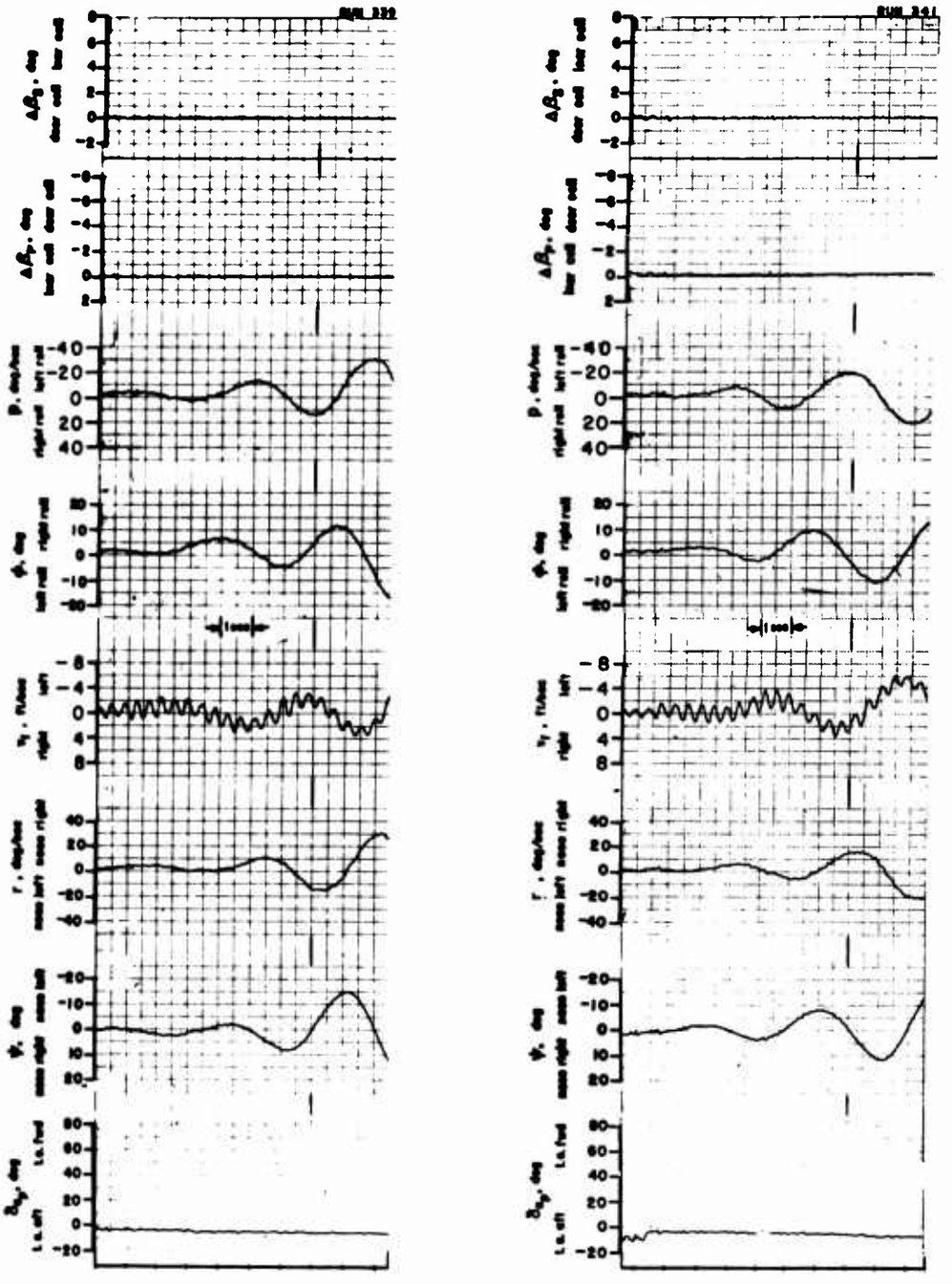

Figure 38. Dynamic Test Data; Lateral/Directional Transient Response. Three Degrees of Freedom, ϕ-Ψ-v_f.
$\theta = 20^\circ$, $\beta_{.75R} = 11.5^\circ$, $\gamma = -11^\circ$, and $U_f = 23.6$ ft/sec.
$i_w = 40^\circ$, $\delta_f = 60^\circ$, $i_t = 20^\circ$.

LITERATURE CITED

1. Reeder, J. P., HANDLING QUALITIES EXPERIENCE WITH SEVERAL VTOL RESEARCH AIRCRAFT, NASA Conference on V/STOL Aircraft, November 1960.

2. Parlett, L. P., and Kirby, R. H., TEST TECHNIQUES USED BY NASA FOR INVESTIGATION DYNAMIC STABILITY CHARACTERISTICS OF V/STOL MODELS, AIAA Aerodynamic Testing Conference, March 9 - 10, 1964.

3. ESTIMATED FLYING QUALITIES XC-142A V/STOL ASSAULT TRANSPORT, Report No. 2-53310/4R939, LTV Vought Aeronautics Division, Dallas, Texas, May 1964.

4. Leppert, D. S., MODEL XC-142A AIRCRAFT FLIGHT TEST, BIWEEKLY SUMMARY REPORT NO. 10, LTV Vought Aeronautics Division, Dallas, Texas, March 15, 1965.

5. Mitchell, R. G., FULL SCALE WIND TUNNEL TESTS OF THE VZ-2 VTOL AIRPLANE WITH PARTICULAR REFERENCE TO WING STALL PHENOMENA, NASA TN-D-2013, December 1963.

6. Goodson, Kenneth W., LONGITUDINAL AERODYNAMIC CHARACTERISTICS OF A FLAPPED TILT-WING FOUR-PROPELLER V/STOL TRANSPORT MODEL, NASA TN-D-3217, Langley Research Center, Langley Station, Hampton, Virginia, March 1966.

7. Boyden, R. P., and Curtiss, H. C., INVESTIGATION OF THE LATERAL/ DIRECTIONAL STABILITY CHARACTERISTICS OF A FOUR-PROPELLER TILT-WING VTOL MODEL, Princeton University; USAAVLABS Technical Report 68-19, U. S. Army Aviation Materiel Laboratories, Fort Eustis, Virginia, April 1968.

8. Curtiss, H. C., Putman, W. F., and Traybar, J. J., GENERAL DESCRIPTION OF THE PRINCETON DYNAMIC MODEL TRACK, Princeton University; USAAVLABS Technical Report 66-73, U. S. Army Aviation Materiel Laboratories, Fort Eustis, Virginia, November 1966, AD 645 883.

9. Curtiss, H. C., AN INVESTIGATION OF THE DYNAMIC STABILITY CHARACTERISTICS OF A QUAD CONFIGURATION DUCTED-PROPELLER V/STOL MODEL, Princeton University; USAAVLABS Technical Report 68-49D, U. S. Army Aviation Materiel Laboratories, Fort Eustis, Virginia, to be published.

10. Seckel, Edward, STABILITY AND CONTROL OF AIRPLANES AND HELICOPTERS, New York, Academic Press, 1964.

APPENDIX
EQUATIONS OF MOTION

Body-Axis System

Linearized equations of motion applicable to the analysis of various experimentally measured responses are presented in this appendix.

The lateral/directional equations of motion that describe the small perturbation motion of an aircraft from initially level flight are (Reference 10)

$$\begin{aligned} \dot{v} - Y_v v + U_o r - g\phi - W_o p &= 0 \\ - L_v v - L_r r + \dot{p} - L_p p &= 0 \\ - N_v v + \dot{r} - N_r r - N_p p &= 0 \end{aligned} \tag{1}$$

These equations are written with respect to principal axes, inclined to the horizon by an angle ζ (Figure 39).

The gimbal mount supporting the model provides pitch freedom about the principal body axis (Y") and yaw freedom about a space-fixed axis ($\bar{Z}_f$), as shown in Figure 39. The relationships between the principal axis angular rates (p,q,r) and the gimbal axis rates ($\dot{\phi},\dot{\theta},\dot{\Psi}$) are

$$\begin{aligned} p &= \dot{\phi} \cos \zeta - \dot{\Psi} \sin \zeta \cos \phi \\ q &= \dot{\theta} + \dot{\Psi} \sin \phi \\ r &= \dot{\Psi} \cos \phi \cos \zeta + \dot{\phi} \sin \zeta \end{aligned} \tag{2}$$

where the order of rotation is (as shown in Figure 40):

1. rotate through Ψ about Z_f axis,
2. rotate through ϕ about X' axis, and
3. rotate through ζ about Y" axis.

For small perturbations in the lateral/directional degrees of freedom and neglecting second-order terms, these equations reduce to

$$\begin{aligned} p &= \dot{\phi} \cos \zeta - \dot{\Psi} \sin \zeta \\ q &= \dot{\theta} \\ r &= \dot{\Psi} \cos \zeta + \dot{\phi} \sin \zeta \end{aligned} \tag{3}$$

It is convenient to transform the velocities to a space-fixed system to correspond to the manner in which the data are presented. The transformation equations for the linear velocities are, from Figure 40,

$$U = U_f (\cos \Psi \cos \zeta - \sin \Psi \sin \phi \sin \zeta) + V_f (\sin \Psi \cos \zeta + \cos \Psi \sin \phi \sin \zeta) - W_f \cos \phi \sin \zeta$$

$$V = -U_f \sin \Psi \cos \phi + V_f \cos \Psi \cos \phi + W_f \sin \phi$$

$$W = U_f (\sin \Psi \sin \phi \cos \zeta + \cos \Psi \sin \zeta) - V_f (\cos \Psi \sin \phi \cos \zeta - \sin \Psi \sin \zeta) + W_f \cos \phi \cos \zeta \quad (4)$$

For small perturbations about a simulated descending flight condition and neglecting second-order terms, these equations reduce to

$$U = U_f \cos \zeta - w_f \sin \zeta$$

$$V = -U_{o_f} \Psi + v_f$$

$$W = U_f \sin \zeta + w_f \cos \zeta \quad (5)$$

Restricting the perturbation degrees of freedom to motions along the Y_f axis and about the X" and $\bar{Z}_f$ axes (as considered in this report) and noting that U_{o_f} is nonzero, these expressions further reduce to

$$U = U_{o_f} \cos \zeta$$

$$V = v_f - U_{o_f} \Psi$$

$$W = U_{o_f} \sin \zeta = W_o \quad (6)$$

Note that W_o is the same W_o that appears as the coefficient of p in the Y-force expression of Equations (1).

Substituting the Equations (3) and (6) into (1),

$$\dot{v}_f - (v_f - U_{o_f}\,\psi)\,Y_v - g\phi = 0$$

$$- L_v\,v_f + U_{o_f}\,L_v\,\psi + (L_p \sin\zeta - L_r\cos\zeta)\,\dot{\psi} - \ddot{\psi}\sin\zeta$$

$$- (L_r \sin\zeta + L_p\cos\zeta)\,\dot{\phi} + \ddot{\phi}\cos\zeta = 0$$

$$- N_v\,v_f + N_v\,U_{o_f}\,\psi + (N_p \sin\zeta - N_r\cos\zeta)\,\dot{\psi} + \ddot{\psi}\cos\zeta$$

$$- (N_r \sin\zeta + N_p\cos\zeta)\,\dot{\phi} + \ddot{\phi}\sin\zeta = 0 \qquad (7)$$

Equations (7) must be modified to account for the "non-lifted" mass of the model support and gimbal system (Figure 7) that translates laterally with the model but is not included in the flying weight. If we define a "lifted" mass m, equal to the resultant aerodynamic force, F, divided by g ($m = \frac{F}{g}$), and a total translating mass, m_t, equal to the sum of the pivoting mass, m_p, and the laterally translating mass, m_ℓ, ($m_t = m_p + m_\ell$), then Equations (7) may be modified by the ratio m/m_t.

In addition, for some single-degree-of-freedom tests, a term must be included to accommodate the effect of the mechanical springs employed to make these motions oscillatory. This term is

$$\Delta N_{\psi_m} = \frac{k_\psi m}{I_z}$$

and its magnitude is given in Table I.

With these modifications, Equations (7) can be rewritten as follows.

$$\dot{v}_f - \frac{m}{m_t}(v_f - U_{o_f}\,\psi)\,Y_v - \frac{m}{m_t}\,g\phi = 0$$

$$- L_v\,v_f + U_{o_f}\,L_v\,\psi + (L_p \sin\zeta - L_r\cos\zeta)\,\dot{\psi} - \ddot{\psi}\sin\zeta$$

$$- (L_r \sin\zeta + L_p\cos\zeta)\,\dot{\phi} + \ddot{\phi}\cos\zeta = 0$$

$$- N_v\,v_f + (N_v\,U_{o_f} + \Delta N_{\psi_m})\,\psi + (N_p \sin\zeta - N_r\cos\zeta)\,\dot{\psi} + \ddot{\psi}\cos\zeta$$

$$- (N_r \sin\zeta + N_p\cos\zeta)\,\dot{\phi} + \ddot{\phi}\sin\zeta = 0 \qquad (8)$$

Gimbal Axis System

To interpret the experimental results it is convenient to rewrite the lateral/directional equations of motion in the axis system of measurement. The resulting expressions describe the motion of the model in terms of forces along the X_f, Y_f, and Z_f axes, and moments about the Z_f, X', and Y" (gimbal) axes. With the principal axis aligned with the horizontal fuselage reference axis, and assuming small perturbation lateral/directional motions, the linearized equations of motion about the space/gimbal axis system are

$$
\begin{aligned}
&-\frac{m_t}{m}\dot{v}_f + Y_v v_f + (\cos\gamma)\, g\phi + (g\sin\gamma - Y_v U_{o_f})\,\Psi = 0 \\
&-I_x'\ddot{\phi} - I_{xz}'\ddot{\Psi} + L_{\dot{\phi}}\dot{\phi} + L_{\dot{\Psi}}\dot{\Psi} + L_{v_f}(v_f - U_{o_f}\Psi) = 0 \qquad (9) \\
&-I_z'\ddot{\Psi} - I_{xz}'\ddot{\phi} + N_{\dot{\phi}}\dot{\phi} + N_{\dot{\Psi}}\dot{\Psi} + N_{v_f}(v_f - U_{o_f}\Psi) = 0
\end{aligned}
$$

where

$$
\begin{aligned}
L_{\dot{\phi}} &= I_x(L_p\cos^2\theta + L_r\sin\theta\cos\theta) \\
&\quad + I_z(N_p\cos\theta\sin\theta + N_r\sin^2\theta) \\
L_{\dot{\Psi}} &= I_x(-L_p\sin\theta\cos\theta + L_r\cos^2\theta) \\
&\quad + I_z(-N_p\sin^2\theta + N_r\sin\theta\cos\theta) \\
L_{v_f} &= I_x L_v\cos\theta + I_z N_v\sin\theta \qquad (10) \\
N_{\dot{\phi}} &= I_z(N_p\cos^2\theta + N_r\sin\theta\cos\theta) \\
&\quad - I_x(L_p\sin\theta\cos\theta + L_r\sin^2\theta) \\
N_{\dot{\Psi}} &= I_z(-N_p\sin\theta\cos\theta + N_r\cos^2\theta) \\
&\quad + I_x(-L_p\sin^2\theta - L_r\sin\theta\cos\theta)
\end{aligned}
$$

and

$$
N_{v_f} = -I_x L_v\sin\theta + I_z N_v\cos\theta.
$$

These equations describe the lateral/directional motions of the model in terms of the measured data quantities. The correspondence between model and full-scale flight conditions is represented in Figure 41.

- Limited Degree of Freedom

When only limited degrees of lateral/directional motion are allowed, Equations (9) can be restricted and simplified as follows:

1. In two degrees of freedom, with $^{k}\Psi_{m} = 0$:

(a) ϕ, v_f ($\Psi = 0$)

$$- \frac{m_t}{m} \dot{v}_f + Y_v v_f + (\cos \gamma) g\phi = 0$$

$$- I_x' \ddot{\phi} + L_{\dot{\phi}} \dot{\phi} + L_{v_f} v_f = 0 \qquad (11)$$

(b) ϕ, Ψ ($v_f = 0$)

$$- I_x' \ddot{\phi} - I_{xz}' \ddot{\Psi} + L_{\dot{\phi}} \dot{\phi} + L_{\dot{\Psi}} \dot{\Psi} - L_{v_f} U_{o_f} \Psi = 0$$

$$- I_z' \ddot{\Psi} - I_{xz}' \ddot{\phi} + N_{\dot{\phi}} \dot{\phi} + N_{\dot{\Psi}} \dot{\Psi} - N_{v_f} U_{o_f} \Psi = 0 \qquad (12)$$

2. Single degree of freedom (with proper value of ΔN_{Ψ_m} from Table I):

$$- I_z' \ddot{\Psi} + N_{\dot{\Psi}} \dot{\Psi} + \Delta N_{\Psi_m} \Psi = 0 \qquad (13)$$

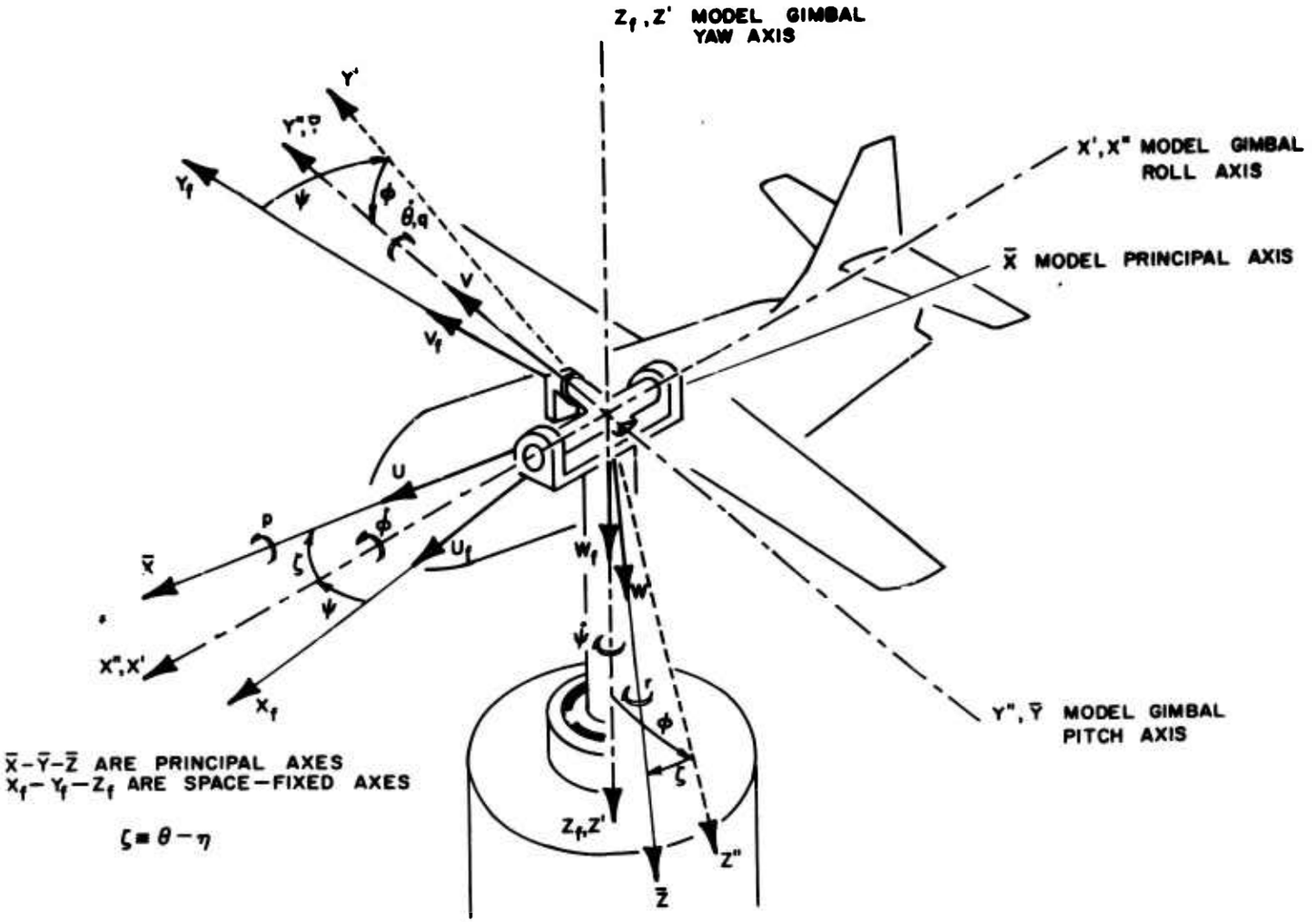

Figure 39. Model Axes Systems and Variables for Lateral/Directional Descent Tests.

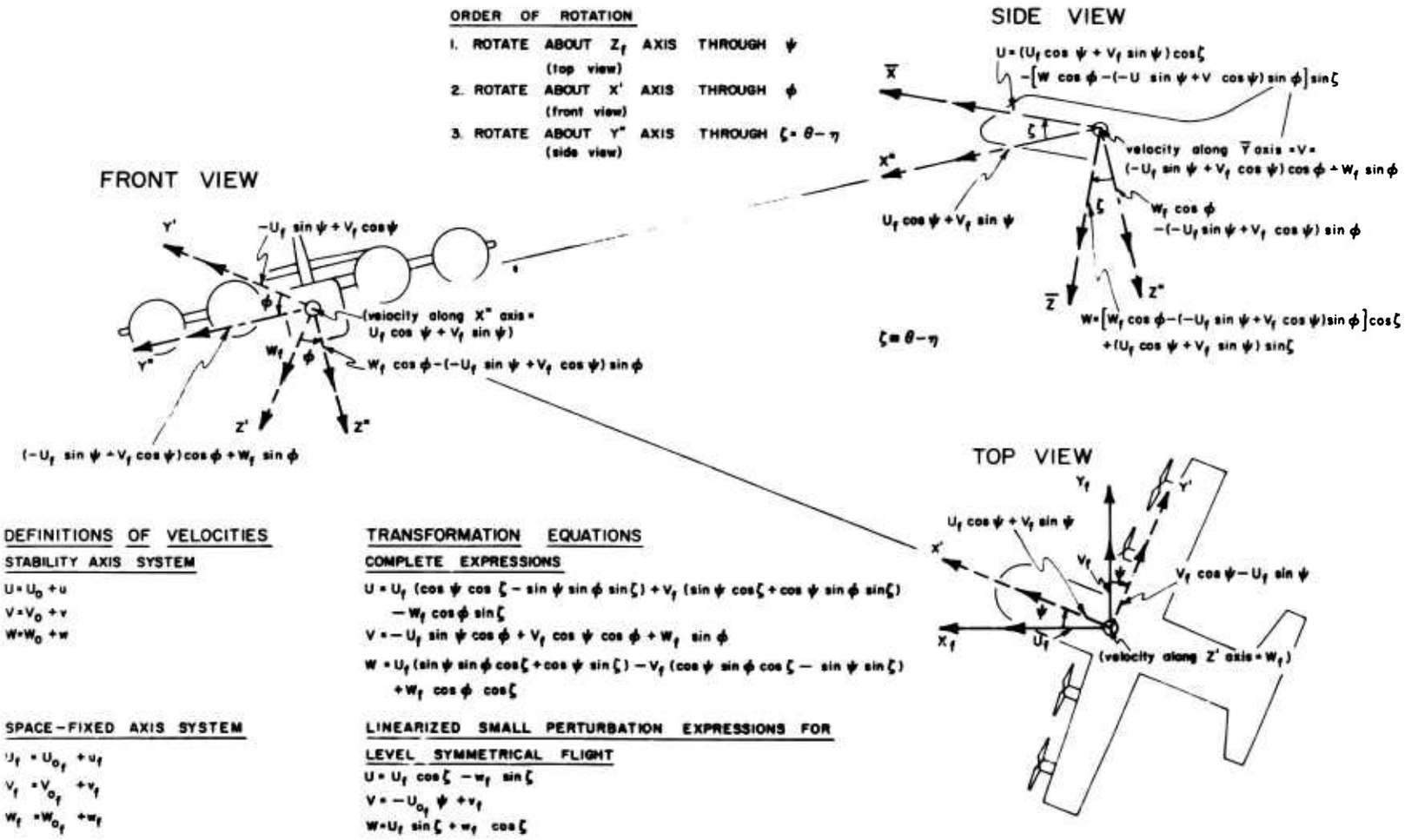

Figure 40. Transformation of Linear Velocities From Space-Fixed to Stability Axis System for Tilt-Wing Model Gimbal System.

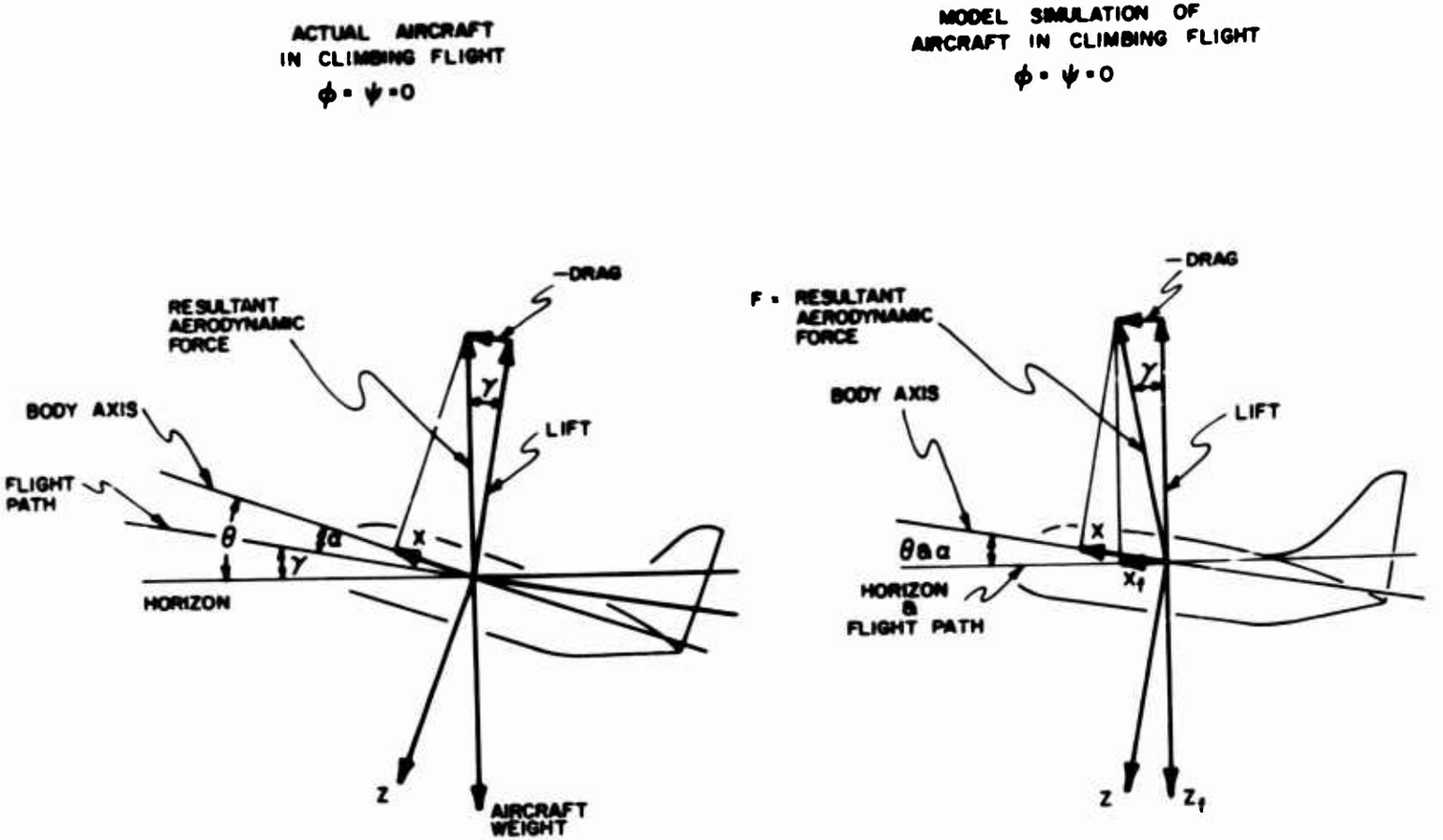

Figure 41. Correspondence of Model and Full-Scale Climbing or Descending Flight Conditions.

Unclassified

Security Classification

DOCUMENT CONTROL DATA - R & D

(Security classification of title, body of abstract and indexing annotation must be entered when the overall report is classified)

1. ORIGINATING ACTIVITY (Corporate author)	2a. REPORT SECURITY CLASSIFICATION
Department of Aerospace and Mechanical Sciences Princeton University Princeton, New Jersey	Unclassified 2b. GROUP

3. REPORT TITLE

An Investigation of the Lateral/Directional Dynamic Stability Characteristics of a Tilt-Wing V/STOL Transport Model in Simulated Low-Speed Descending Flight

4. DESCRIPTIVE NOTES (Type of report and inclusive dates)

Final Data Report

5. AUTHOR(S) (First name, middle initial, last name)

William F. Putman

6. REPORT DATE	7a. TOTAL NO. OF PAGES	7b. NO. OF REFS
July 1969	75	10

8a. CONTRACT OR GRANT NO.	9a. ORIGINATOR'S REPORT NUMBER(S)
DAAJ02-67-C-0025 b. PROJECT NO. Task 1F162204A14233	USAAVLABS Technical Report 69-46
c. d.	9b. OTHER REPORT NO(S) (Any other numbers that may be assigned this report) Aerospace Sciences Report 862

10. DISTRIBUTION STATEMENT

This document is subject to special export controls and each transmittal to foreign governments or foreign nationals may be made only with prior approval of US Army Aviation Materiel Laboratories, Fort Eustis, Virginia 23604.

11. SUPPLEMENTARY NOTES	12. SPONSORING MILITARY ACTIVITY
	U. S. Army Aviation Materiel Laboratories Fort Eustis, Virginia

13. ABSTRACT This report represents the results of an experimental program to measure the lateral/directional dynamic stability characteristics of a tilt-wing V/STOL transport model in simulated descending flight. A 0.1-scale dynamically similar model of the XC-142A V/STOL aircraft was tested on the Princeton Dynamic Model Track in the three degrees of lateral/directional freedom: roll, yaw, and sideslip. The test conditions simulated a full-scale aircraft with wing loading of 70 pounds per square foot (gross weight = 37,400 pounds), flying at approximately 40 knots at a wing incidence of 40 degrees and flap deflection of 60 degrees. The simulated descent conditions encompassed level flight and four sink rates up to approximately 1,000 feet per minute equivalent full-scale sink rate.

Time histories of the lateral/directional transient response of the model in one, two, and three degrees of freedom were measured. Pursuant to these experiments, the aerodynamic forces and moments acting on the model were measured as functions of the flight variables and model control displacements. The results of these tests defined the descent trim conditions and determined the model control effectiveness and control mixing requirements for this mid-transition flight condition.

Throughout the lateral/directional dynamic test program, the model was stability-augmented in pitching freedom only. A pitch attitude-hold loop, employing pitch rate, pitch attitude, and integral of pitch attitude feedback signals, was used to insure that no spurious lateral/directional motions would occur in the axis system of measurement due to untrimmed body-axis pitching moments. Earlier studies of the lateral/directional motions of this aircraft had indicated the necessity of such a pitch-trim system.

DD FORM 1 NOV 1473 REPLACES DD FORM 1473, 1 JAN 64, WHICH IS OBSOLETE FOR ARMY USE.

Unclassified

Security Classification

Unclassified

Security Classification

14. KEY WORDS	LINK A		LINK B		LINK C	
	ROLE	WT	ROLE	WT	ROLE	WT
V/STOL						
DYNAMIC STABILITY						
LATERAL/DIRECTIONAL STABILITY						
XC-142A TILT WING						
DESCENDING FLIGHT						

Unclassified

Security Classification

7076-69